BRNO UNIVERSITY OF TECHNOLOGY

Faculty of Electrical Engineering
and Communication

MASTER'S THESIS

Brno, 2020 Bc. Jakub Lázňovský

BRNO UNIVERSITY OF TECHNOLOGY
VYSOKÉ UČENÍ TECHNICKÉ V BRNĚ

FACULTY OF ELECTRICAL ENGINEERING AND COMMUNICATION
FAKULTA ELEKTROTECHNIKY
A KOMUNIKAČNÍCH TECHNOLOGIÍ

DEPARTMENT OF BIOMEDICAL ENGINEERING
ÚSTAV BIOMEDICÍNSKÉHO INŽENÝRSTVÍ

AIRWAY ANALYSIS OF PREMATURELY BORN BABIES BASED ON X-RAY CT AND MRI SCANS
ANALÝZA DÝCHACÍCH CEST PŘEDČASNĚ NAROZENÝCH DĚTÍ NA ZÁKLADĚ MRI A CT DAT

MASTER'S THESIS
DIPLOMOVÁ PRÁCE

AUTHOR — **Bc. Jakub Lázňovský**
AUTOR PRÁCE

SUPERVISOR — **Ing. Jiří Chmelík**
VEDOUCÍ PRÁCE

BRNO 2020

BRNO UNIVERSITY OF TECHNOLOGY
FACULTY OF ELECTRICAL ENGINEERING AND COMMUNICATION

Master's Thesis

Master's study program **Biomedical Engineering and Bioinformatics**

Department of Biomedical Engineering

Student: Bc. Jakub Lázňovský ***ID:*** 186673

Year of study: 2 ***Academic year:*** 2019/20

TITLE OF THESIS:

Airway analysis of prematurely born babies based on X-ray CT and MRI scans

INSTRUCTION:

1) Elaborate a literary research in the field of anatomy, physiology and pathologies of airways with focus on child airway, in the field of pulmonary modeling and its application and in the field of used imaging modalities.
2) Get acquainted with the measured data and segment the airways using a suitable method. 3) Propose and test a method for creating a representative airway model. 4) Create a representative newborn airway model. 5) Propose a methodology for the analysis of the created airway model and suggest suitable evaluation parameters. 6) Evaluate selected parameters of the airway model and discuss the accuracy of the analysis.

RECOMMENDED LITERATURE:

[1] JAN, J. Medical image processing, reconstruction and restoration: concepts and methods. Boca Raton: Taylor, 2006, 730 s. ISBN 08-247-5849-8.

[2] KAK, A. C., M. SLANEY a G. WANG. Principles of Computerized Tomographic Imaging. Medical Physics. 2002, 29(1), 107-107. DOI: 10.1118/1.1455742. ISSN 00942405.

[3] SUN, S., C. BAUER a R. BEICHEL. Automated 3-D Segmentation of Lungs With Lung Cancer in CT Data Using a Novel Robust Active Shape Model Approach. IEEE Transactions on Medical Imaging. 2012, 31(2), 449-460. DOI: 10.1109/TMI.2011.2171357. ISSN 0278-0062.

Date of project specification: 3.2.2020 ***Deadline for submission:*** 29.5.2020

Supervisor: Ing. Jiří Chmelík
Consultant: Ing. Adam Břínek

prof. Ing. Ivo Provazník, Ph.D.
Chair of study program board

ABSTRACT

The proposed Master's thesis deals with the analysis and creation of airway models of premature babies. Firstly, the theoretical basis is discussed in the field of development of the respiratory system and the creation of airway models. Then the used imaging modalities are introduced, and methods for working with image data are described. The practical part of the thesis deals with the creation of airway models of three newborns. All of these models are based on clinical CT and MRI data of neonates born at 30 weeks of gestational age. In these created models, selected parameters related to the anatomical structure of the airways are further analysed. Based on the analysis of these parameters, a representative model corresponding to the airways of a newborn of a given gestational age was subsequently proposed.

KEYWORDS

Airway model, Neonatology, Medical imaging, Image processing

ABSTRAKT

Předkládaná Diplomová práce se zabývá analýzou a tvorbou modelů dýchacích cest předčasně narozených dětí. Nejprve je položen teoretický základ v oblasti vývoje dýchacího ústrojí a tvorby modelů dýchacích cest. Poté jsou představeny využité zobrazovací modality a popsány metody pro práci s obrazovými daty. Praktická část práce se zabývá vytvořením modelů dýchacích cest tří novorozenců. Všechny tyto modely jsou vytvořeny na základě klinických CT a MRI dat novorozenců narozených ve 30. týdnu gestačního věku. U těchto vytvořených modelů jsou dále analyzovány vybrané parametry související s anatomickou strukturou dýchacích cest. Na základě analýzy těchto parametrů byl následně navrhnut reprezentativní model, odpovídající dýchacím cestám novorozence daného gestačního věku.

KLÍČOVÁ SLOVA

Model dýchacích cest, Neonatologie, Lékařské zobrazovací metody, Zpracování obrazů

LAZNOVSKY, Jakub. *Airway analysis of prematurely born babies based on X-ray CT and MRI scans*. Brno, 2020, 72 p. Semestral project. Brno University of Technology, Fakulta elektrotechniky a komunikačních technologií, Ústav biomedicínského inženýrství. Advised by Ing. Jiří Chmelík, Consultant: Ing. Adam Břínek

ROZŠÍŘENÝ ABSTRAKT

Úvod

Předkládaná diplomová práce se zabývá vytvořením reprezentativního modelu dýchacích cest předčasně narozených dětí. Model je vytvořen na základě získaných klinických CT a MRI dat.

V první části je obecně popsána problematika spojená s tvorbou modelů. Nejprve je popsána dýchací soustava člověka, se zaměřením na její vývoj a možné problémy při vývoji u předčasně narozených dětí. Stručně jsou také popsány možnosti léčby těchto vývojových poruch a možnosti plicní ventilace, která bývá s těmito problémy často spojena. Další část práce se věnuje akvizici CT a MRI dat, na základě kterých byl tento model vytvořen. Jsou zde vysvětleny principy obou využitých zobrazovacích metod a možnosti akvizice dat. Ve třetí kapitole jsou popsány způsoby tvorby geometrie plicních modelů a jejich následná charakteristika a využití. Ve čtvrté kapitole jsou popsány metody zpracování obrazů. Jedná se zejména o rešerši přístupů pro segmentaci dýchacích cest a hodnocení kvality této segmentace. Následuje praktická část diplomové práce.

Popis řešení

Pro vytvoření reprezentativního modelu jsou využita dostupná klinická data z CT a MRI zobrazovacích technik. Jedná se konkrétně o MRI hlavy, kde jsou zobrazeny horní cesty dýchací a CT plic, kde je zachycena informace o dolních cestách dýchacích. Bohužel žádný z dostupných datasetů neobsahuje informaci o celých dýchacích cestách. Z tohoto důvodu je nutná následná registrace těchto datasetů pro vytvoření jednoho partikulárního modelu.

Cílem této práce je vytvořit jeden reprezentativní model. Pro jeho tvorbu byly využity informace ze tří partikulárních modelů. Tyto modely byly získány na základě vytvořeného algoritmu. Následná analýza těchto modelů získá data pro popis parametrů modelu reprezentativního.

Nejprve byla vybrána vhodná data. Z dostupných datasetů byly vyřazeny ty, které nesplňovaly požadavky na minimální obrazovou kvalitu. Ze zbylých datasetů byly vybrány ty, kde měření odpovídá novorozencům narozeným ve stejném gestačním týdnu a skenovaným ve stejné době po porodu. Jako reference pro tato kritéria byly použity MRI skeny hlavy, kde je jasně určen gestační, i poporodní věk. CT data plic jsou získána z předčasně narozených novorozenců, kde je ale znám pouze poporodní věk. Výběr vhodného datasetu dolních cest dýchacích pro kombinaci s horními dýchacími cestami je založen na analýze průměrů průdušnice. Tyto průměry byly měřeny na třech přibliženě odpovídajících řezech v objemu. K horním cestám dýchacím byl vybrán takový dataset, kde průměr průdušnice byl nejpodob-

nější. Rozdíly v těchto průměrech se liší pouze sub-voxelově, tudíž mají na výsledný model zanedbatelný vliv.

V další části jsou vybraná data předzpracována pro dosažení lepších výsledků následné segmentace. Samotné předzpracování se skládá ze tří kroků. Nejprve jsou data podvzorkována na izotropickou velikost voxelu 0,2 mm. Tato hodnota byla zvolena jako kompromis mezi rozumnou velikostí celého datového objemu a dostatečnou redukcí schodovitého artefaktu, který vzniká kvůli velké velikosti voxelu v transverzální rovině. Pro převzorkování byla využita kubická interpolace. Dále je využit bilaterální filtr, který obraz vyhladí, ale zároveň zachová hrany v obraze. Optimalizace parametrů bilaterálního filtru byla provedena na základě porovnání vybraných parametrů mezi originálním a filtovaným obrazem.

Segmentace předzpracovaných dat je klíčová pro vytvoření validního modelu. Pro tuto úlohu je využita modifikovaná matoda narůstání oblastí. Nejprve je automaticky zvoleno iniciační semínko na základě průměrné intenzity v masce. Místo, kde je průměrná intenzita nejnižší, odpovídá nejširší části průdušnice. Dále probíhá rozrůstání oblasti v 6-okolí iniciačního semínka, a na základě rozptylu v 26-ti okolí tohoto semínka je zajišťována detekce úniku segmentu mimo dýchací cesty. Tento princip segmentace je ovšem účinný pouze do průměru vnitřních struktur o velikosti 1,5 mm. Z tohoto důvodu je nutná následná manuální korekce, při které jsou k segmentu přidány tenčí bronchioly a místa s nižším kontrastem, zejména v horních cestách dýchacích.

Další část algoritmu provádí předregistrování obou datasetů pro následnou finální manuální registraci. Tato předregistrace je založena na detekci centroidů průdušnic v obou datasetech. Na základě pozic centroidů je vysegmentovaná maska horních cest dýchacích ve svém objemu posunuta tak, že se centroidy obou průdušnic překrývají. Tento krok usnadňuje následné manuální zarovnání, které probíhá v programu Avizo. Výsledkem je vytvoření partikulárního modelu, který je založen na kombinaci těchto dvou datasetů.

Výše popsaným způsobem jsou vytvořeny tři partikulární modely. Tyto modely jsou následně analyzovány pro zjištění jejich anatomických parametrů. Bylo vybráno dvanáct parametrů, na základě kterých je možné definovat reprezentativní model. Většina těchto parametrů je získána díky rozdělení modelu na jednotlivé oblasti zájmu. Toto rozdělení je založeno na skeletonizaci, následný převod na grafovou reprezentaci skeletonu a poté na detekci klíčových bodů v grafu. Tímto způsobem jsou detekována místa, kde začíná a končí průdušnice, a kde končí hlavní průdušky. Pomocí těchto klíčových bodů je možné model rozdělit na jednotlivé oblasti zájmu, ve kterých jsou následně analyzovány hodnocené parametry.

Na základě tohoto postupu jsou analyzovány všechny tři partikulární modely. Vypočítané parametry charakterizující tyto modely jsou následně zprůměrovány.

Průměr těchto parametrů tvoří reprezentativní model. Pro ověření, zda jsou všechny parametry validní, byla provedena jejich standardizace směrodatnou odchylkou a výsledná hodnota z-skóre byla vynesena do grafu. Na základě validace směrodatnou odchylkou lze konstatovat, že všechny parametry všech partikulárních modelů jsou validní, tudíž z nich lze vytvořit model reprezentativní.

V další části práce je popsána tvorba semirealistické geometrie dýchacích cest na základě vytvořeného parametrického modelu. Horní cesty dýchací této geometrie jsou vytvořené z modelu číslo 2, který v této oblasti nejvíce odpovídal modelu reprezentativnímu. Dolní cesty dýchací jsou vytvořeny z trubic, jejichž parametry (průměry a délky) odpovídají parametrům průdušnice a průdušek v reprezentativním modelu.

V poslední části práce je diskutována přesnost získaného parametrického modelu. Přesnost je závislá na třech faktorech: počet partikulárních modelů, kvalita segmentace a přesnost hodnocení parametrů. Celková přesnost je dána všemi třemi faktory dohromady.

Shrnutí výsledků

Cílem práce bylo vytvořit reprezentativní model dýchacích cest předčasně narozených dětí. Pro tento účel byl vytvořen postup, díky kterému jsou na základě MRI a CT dat získány tři partikuálrní modely dýchacích cest. Tyto modely byly analyzovány a díky získaným parametrům byl popsán parametrický reprezentativní model. Tento model odpovídá dýchacím cestám novorozence narozeného ve 30. týdnu gestačního věku sterému dva týdny. Na základě parametrů, kterými je reprezentativní model popsán, byla vytvořena semirealistická geometrie těchto dýchacích cest. Geometrie byla následně exportována ve formátu *.stl*, který je vhodný pro výrobu prototypů pomocí 3D tisku. Na konci práce je poté diskutována celková reprezentativnost vytvořeného parametrického modelu.

DECLARATION

I declare that I have written the Master's Thesis titled "Airway analysis of prematurely born babies based on X-ray CT and MRI scans" independently, under the guidance of the advisor and using exclusively the technical references and other sources of information cited in the thesis and listed in the comprehensive bibliography at the end of the thesis.

As the author I furthermore declare that, with respect to the creation of this Master's Thesis, I have not infringed any copyright or violated anyone's personal and/or ownership rights. In this context, I am fully aware of the consequences of breaking Regulation § 11 of the Copyright Act No. 121/2000 Coll. of the Czech Republic, as amended, and of any breach of rights related to intellectual property or introduced within amendments to relevant Acts such as the Intellectual Property Act or the Criminal Code, Act No. 40/2009 Coll., Section 2, Head VI, Part 4.

Brno ....

author's signature

ACKNOWLEDGEMENT

I would like to thank my supervisor, Ing. Jiří Chmelík for his professional leadership, for practical methodological and expert assistance, and other valuable advice in the creation of my Master's thesis. I would also like to thank my consultant, Ing. Adam Břínek for helpful consultations in the field of image data processing and the thesis structure.

Brno ....

author's signature

Contents

List of Figures

List of Tables

Introduction

Insufficient lung development is still the highest mortality factor in prematurely born babies. Fortunately, there are breathing support devices which help infants to endure the critical phase of lung development. However, neonatologists often struggle with the correct settings of the breathing support devices to provide maximum possible breathing support.

The correct settings of breathing support devices can be tested on the models corresponding to the airways of newborns in a particular stage of development. Such testing can lead to a better understanding of air behaviour in newborns airways. Parameters describing air behaviour in airways models are calculated based on pressure fields and gas flow rates (described in Chapter 3).

The practical part of this thesis is devoted to the representative newborn's airways model description and construction. The description is based on MRI (Magnetic Resonance Imaging) and X-Ray CT (X–Ray Computed Tomography) scans. These available scans were performed as a part of diagnostic measurements of newborns. In particular, MRI sequences were performed to examine the brain, and CT scans were performed to visualize the lungs. There is unfortunately no available dataset containing both, upper and lower airways in one continuous scan.

To ensure the representativeness of the model, all pathologies and scanning artifacts have to be avoided. Therefore, the representative airway model was created from three particular airway models. At first, it is necessary to segment the airways. Infants' airway segmentation is a challenging task due to insufficient data quality for segmentation methods which are effective in adult airway segmentation. Based on literary research, a modified region-growing approach was chosen to deal with this issue partially. Subsequently, both datasets containing the airways (CT and MRI) are registered to create one particular airway model. In this manner, three particular models were created.

A further step for the development of the representative model is obtaining the parameters which describe its geometry. For this purposes were chosen several parameters corresponding to the anatomy of infant's airways, which were evaluated in particular models. These parameters were consequently averaged, where the average describes the representative model. This model is therefore described parametrically, and based on these parameters was constructed semirealistic model geometry. The resulting airway geometry was consequently exported in *.stl* format.

The final part of this thesis is devoted to the statistical analysis of the obtained parameters. These parameters were depicted as a z-score which proves the competence of particular models to contribute in the representative model. The z-score calculation is based on the standard deviation of individual parameters within all

particular models. The verification proved that all models could contribute to the final geometry of the representative model. The model development accuracy is discussed in the final part of the thesis. The accuracy depends on the number of particular models and the accuracy of segmentation and models analysis.

1 Respiratory system of prematurely born infants

The respiratory tract, lungs and diaphragm do form early in embryonic development. The fundamental structure of respiratory tract starts developing around the 5^{th} week after fertilization. Then in the next few weeks, this structure grows and expands [1]. The respiratory tract is anatomically divided into two main parts:

1. Upper respiratory tract, consisting of the nose, nasal cavity and the pharynx
2. Lower respiratory tract consisting of the larynx, trachea, and the lungs itself

Development of this system is not completed until the last weeks of fetal development. Alveoli are being fully developed just before birth [2]. There are two main respiratory cell types in alveoli. Both arise from the same bi-potential progenitor cell [3]. Squamous alveolar type 1 that form the structure of the alveoli. And than squamous alveolar type 2 that secrete surfactant. Alveolar cells type 2 starts to develop about 26^{th} week of gestation. Therefore premature babies have difficulties associated with insufficient surfactant production. Surfactant is a substance that reduces surface tension in the lungs. It consists of a mixture of phospholipids, proteins and ions. It reduces the surface tension at the boundary of the fluid-air interface in the alveoli. Therefore, it increases lung compliance. The absence or insufficient secretion of surfactant leads to alveoli collapse with subsequent respiratory failure [4].

Premature birth is defined as the birth of a child before the 37^{th} week of gestation. Premature births can be further divided into three subcategories:

- slightly premature - births between 32^{th} and 36^{th} weeks of gestation
- very premature - births between the 28^{th} and 31^{st} weeks of gestation
- extremely premature - deliveries before or during the 27th week of gestation

The lower limit of preterm child delivery in the Czech Republic has been set up for the 24^{th} week. The limit was approved by the Czech Neonatology Society in 1994. This limit may vary in different countries, but there are no significant differences between developed countries [5].

1.1 Anatomy

Development of the nasal cavity is related to the development of the fetus head. Ectodermal tissue invaginates posteriorly to form olfactory pits, which fuse with

endodermal tissue of the developing pharynx. As the fetus develops, the olfactory pit grows, creates a dividing septum and enlarges to become the nasal cavity.

The structure connected to the developing head is a primitive gut tube – the precursor to the gastrointestinal tract. At about the fourth week of development is in the primitive gut tube developed laryngotracheal diverticulum. This diverticulum stands for initiating trachea. The diverticulum expands and creates a tracheal bud, which is in couple days divided into two primary bronchial buds (precursors of bronchial tubes). These bronchial buds are subsequently again divided into secondary bronchi (two for left and three for right lung). Meantime the tracheoesophageal folds (the tissue between trachea and oesophagus) start fusing and create tracheoesophageal septum which divides trachea from the oesophagus – The whole process is depicted in Figure 1.1.

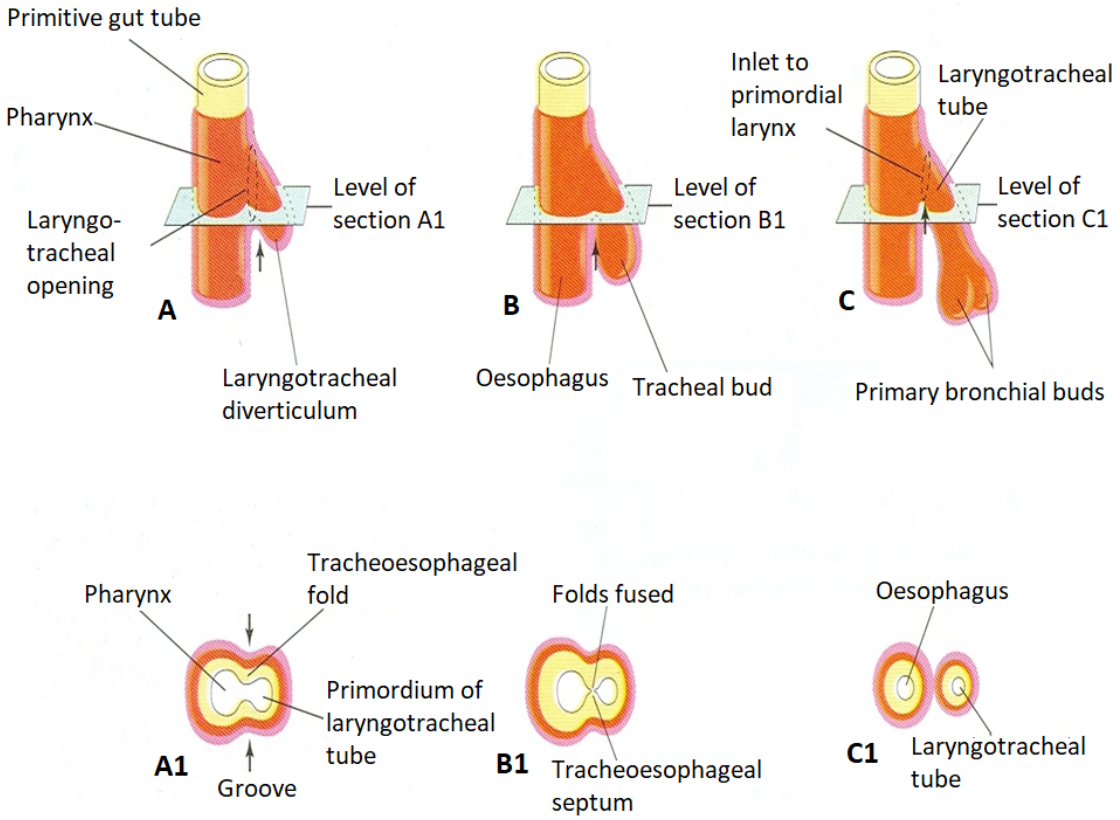

Fig. 1.1: The process of tracheoesophageal septum development. The cross sections in the upper parts corresponds the images in lower part [6].

Development of human lungs can be divided into five stages. Every stage is related to a certain period of development (see Fig.: 1.2). Timing of the development stages is not strict, and it may vary for individuals.

1. **Embryonic stage:** 4–5 week of gestation. The Genesis of tracheal buds – predecessors of main bronchi. See figure 1.1.

2. **Pseudoglanduar stage:** 5–17 week of gestation. Branching bronchi and bronchioles expand in the splanchnic mesenchyma of the pleural cavities.

3. **Canalicular stage:** 16–25 week of gestation. Bronchi and bronchioles widen their diameter. The tissue is being vascularized. The alveolar epithelium starts to develop. At the end of this stage, breathing theoretically possible

4. **Saccular stage:** 24–40 week of gestation. Development of alveolar ducts and air sacs (primitive alveoli). Differentiation of squamous alveolar cell types 1 and cell type 2. Start of the surfactant production.

5. **Alveolar stage:** Late fetal up to 8 years. Capillaries and alveoli increase in the numbers and size. Lung exapnd and the alveoli are filled with the air which gives them the definitive form after birth. In the early years of a child's life, the formation of new alveoli continues.

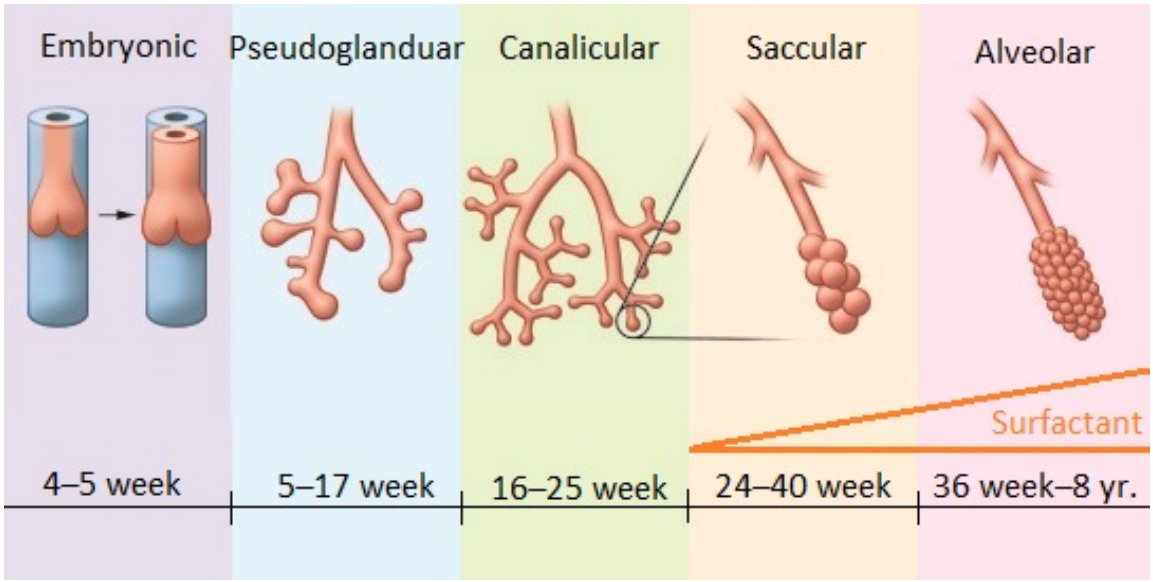

Fig. 1.2: Lung differentiation can be divided into five stages [7]. The surfactant starts to be produced in 24^{th} week of gestation.

The developement of the respiratory tract continues also postnatally. Upper respiratory tract expands its diameter and forms the nasal septum and cavities. The trachea enlarges and widens in its diameter. Approximate length of infant trachea is 4.13 ± 0.53 cm. In the lungs themselves continue the development of the capillary system and the number of alveoli is increased. The newborn's lungs

contain about 20 million alveoli, while the adult's lungs contain about 300 million alveoli [8].

1.2 Physiology

The umbilical cord develops to deliver substances as oxygen directly to the developing fetus's body, after 5-6 weeks of pregnancy [9]. Two separate blood vessels are in umbilical cord, so waste products can separately leave the fetus body. This system of blood exchange lasts until the fetus birth. By approximately 11 weeks of gestation, fetal breathing movements can be detected on ultrasound. The number and duration of movements increase with advancing gestational age. These breathing movements fill the developing lungs with amniotic fluid, which surrounds the fetus in the womb [10]. Inspired amniotic fluid expands the lungs, and influences the lungs formation. Fetal breathing movements also help with the development of respiratory muscles and neural regulation [11].

In healthy development, the amount of produced surfactant increases approximately two weeks before birth. This system helps the lungs to prepare the body for the first breath after birth. The first inhale comes spontaneously due to lack of amniotic fluid and exposure to air. Increased oxygen in the lungs causes a decrease in blood flow resistance to the lungs. Amniotic fluid drains or is absorbed from the respiratory system. The lungs are empty and can be inflated and start working autonomously. Breathed air enters into the upper respiratory tract. Upper respiratory tract conveys, moistens, and warms the air from outside the body as it makes its way to the lungs. In the lungs, oxygen enters into the bloodstream, and carbon dioxide is removed by breathing the air out [12].

1.3 Pathology

Pathological conditions related to lungs development occur significantly and more frequently in premature infants. Premature infants are more likely to face risk factors such as low birth weight, infections, or complications during pregnancy which also affect the lungs development. The risk of respiratory complications decreases with the gestational age of the infant. If premature delivery is suspected, corticosteroids are administered to the mother to prolong pregnancy. Corticosteroids help to speed up the fetus's lung development. The biggest problem of the undeveloped lungs is an insufficient amount of surfactant. Lung bronchioles collapse manifest by increased work of breathing and limitation of the functional residual capacity of the lungs. This condition leads to a low level of oxygen in the bloodstream and

the newborn needs to be ventilated. The conventional solution for these infants is long-term oxygen or breathing support by continuous positive airway pressure CPAP (Continuous Positive Airway Pressure) machines. Another method of treatment is the use of ventilators and medicines like bronchodilators. Infants treated with breathing support may struggle breathing problems throughout childhood and even into adulthood. The following chapters deal with the most common infants' diseases related to lung development.

1.3.1 Infant Respiratory distress syndrome

Infant respiratory distress syndrome (IRDS), also called hyaline membrane disease is a syndrome caused by anatomical and functional immaturity of the lungs. Therefore it most occurs in premature infants affecting nearly all infants born before 28^{th} week of gestational age. The main factor causing this syndrome is the lack of surfactant and structural immaturity of the lungs. Surfactant prevents the air spaces from collapsing on exhalation, by reducing surface tension [4]. Due to lack of surfactant, the alveoli collapse and the infant is not able to reach sufficient pressure to reopen the alveoli. During the alveoli collapse are hyaline membranes collected in the airways. Hyaline membranes are composed of fibrin, cellular debris and red blood cells. They fill the air spaces and blocking gas exchange. Thus, the oxygen level in the blood decreases and carbon dioxide increases. This condition leads to an increase in blood acid level (acidosis) and hypoxia [13] (see Fig.: 1.3).

IRDS usually develops shortly after birth. Main symptoms are tachypnea, dyspnea, tachycardia and grunting (breath against a partially closed glottis which helps to maintain positive airway pressure). The syndrome is more frequent in Caucasians, males, infants of diabetic mothers and the second-born of premature twins. The incidence and severity of IRDS are related inversely proportional to the gestational age of the infant.

The diagnosis of IRDS is evident in most cases according to the appearance and breathing difficulties of the infant. It can be approved by the chest X-ray, which demonstrates decreased lung volumes, reduced lung transparency and absence of the thymus. There are two main methods of treatment (described in more detail in Chapter 1.1.4):

1. Utilization of CPAP (Continuous Positive Airway Pressure)

2. Intra-tracheal apply of a surfactant.

The IRDS can only be prevented to prevent a premature birth. The premature birth is prevented by application of corticosteroids to the mothers' body before the delivery. Corticosteroids prolong the pregnancy and thus lower the risk of preterm

birth.

Despite significant advances in care, IRDS remains the most common single cause of death in the first month of life in the modern healthcare. Even if is IRDS stabilized, it may transform to bronchopulmonary dysplasia over time.

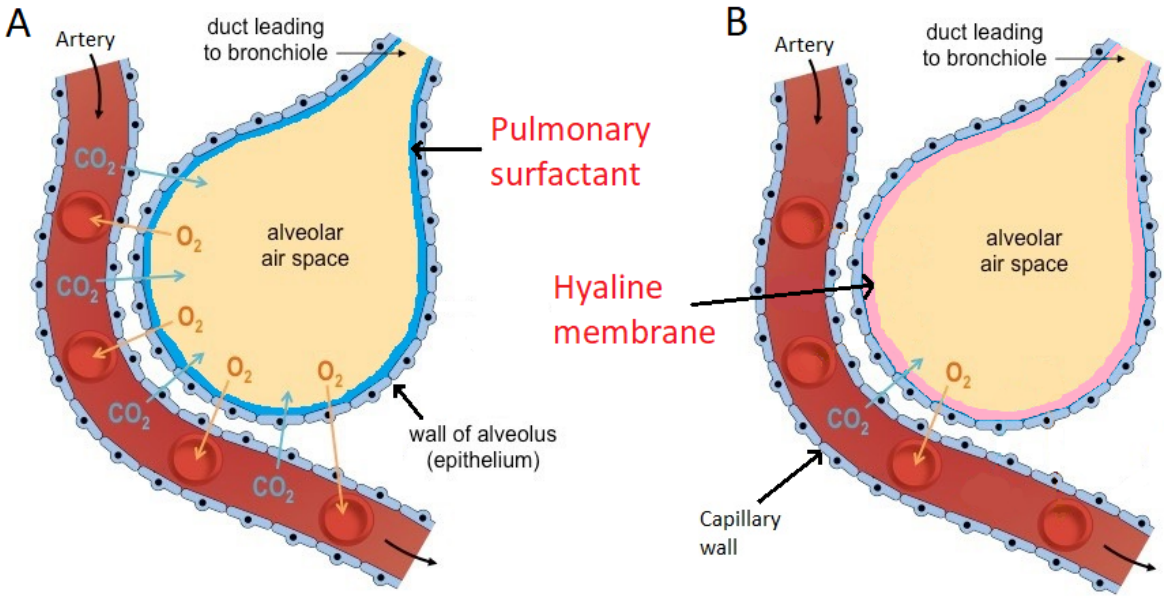

Fig. 1.3: Infant Respiratory distress syndrome [14].

1.3.2 Bronchopulmonary dysplasia

Bronchopulmonary dysplasia (BPD) is a neonatal form of chronic lung involvement. BPD is defined as the persistent dependence of an initially premature newborn on oxygen or ventilation support at 28 days of age [15]. It results from damage to the lungs caused by mechanical ventilation (respirator) and long-term use of oxygen.

It is more frequent in infants who receive prolonged mechanical ventilation to treat respiratory distress syndrome (RDS). BPD is manifested by respiratory distress symptoms. The essence of the problem is the restriction of the respiratory surface of the lungs with an increase in interstitial connective tissue. The treatment includes persistent ventilation support and oxygen therapy, adequate nutrition, and maintaining the internal environment.

During treatment, the protection against respiratory infections and injuries is essential. Damaged lungs develop abnormally, due to the structural changes, such as slowed alveolarization process and pulmonary artery dysgenesis. Lungs affected by BPD have less septum, fewer and larger alveoli, reduced pulmonary capillarization,

which can lead to secondary pulmonary hypertension. Lack of progress may in part be attributed to the limited therapeutic options available for prevention and treatment of BPD [16].

The diagnosis is very similar to RDS. The infants' dependence on respiratory support is assessed. It is crucial to achieving disconnection from respiratory support as soon as possible. Next diagnosis possibilities include lung RTG and blood saturation monitoring. Most infants recover from BPD, but some may have long-term breathing difficulties. These difficulties include asthma-like symptoms and exercise intolerance in young adults.

1.4 Respiratory support

Most of the preterm infants suffer from Infant respiratory distress syndrome. IRDS treatment is based on exogenous surfactant administration which is obtained from other mammal species (porcine, bovine) [17]. This therapy is not always sufficient by itself, and various methods of respiratory support are essential. Although, infants with IRDS are often able to breathe spontaneously, they are not able to ensure sufficient gas exchange. Respiratory support aims to promote adequate oxygenation of the blood and adequate ventilation - excretion of carbon dioxide.

The lungs of very preterm infants are highly susceptible to injury. They are structurally immature, have a lack of surfactant, and they are not supported by a rigid chest wall. Therefore the lungs of preterm infants can be easily damaged by mechanical ventilation. Nevertheless, there is often no alternative than to use respiratory support. Respiratory support can be roughly divided into two main approaches, invasive and non-invasive ventilation.

1.4.1 Invasive ventilation

Invasive ventilation is mechanical breathing support. It is based on positive-pressure ventilation (PPV). The purpose of PPV is to ensure lung aeration, initiate spontaneous breathing and facilitate gas exchange. Using PPV, the tube is inserted into the trachea, via the mouth, alternatively tracheostomy. Mechanical ventilation partly or fully supplies work of breathing. Despite lifesaving in many instances, PPV is very often responsible for lung injuries, through various mechanisms. Possible causations: high airway pressure (barotrauma), high tidal volume (volutrauma), repeated alveolar collapse and reexpansion (atelectrauma), and infection or inflammation [18]. There are many modifications of invasive respiration. In general, these modifications can be divided to controlled ventilation, support ventilation modes and hybrid modes, combining controlled and support ventilation. All these modifications are

based on pressure or volume-controlled ventilation. Maximum set inspiratory pressure or tidal volume is supplied to the lungs. Thereafter, passive expiration occurs to atmospheric pressure or a preset positive pressure that prevents alveoli collapse. Today's strategy of ventilation support prefers non-invasive methods that are more gentle, so infants are preferably treated this way.

1.4.2 Non-invasive respiratory support

Non-invasive respiratory support methods are based on artificially increasing air pressure in the lungs at the end of expiration. Intubation is no longer used, but a respiratory support device is connected directly to the nose via nasal cannula. Therefore, the upper airways also play a role in the delivery of support. Different studies have shown that these therapies can decrease the need for intubation and ventilation, decrease the length of intensive care days, and increase patient comfort [18]. There are two main approaches to non-invasive support:

CPAP – continuous positive airway pressure

This form of respiratory support poses a positive airway pressure continuously administered to the airways. Air is administered to the lungs via the nasal cannula. This creates a pressure increase in the upper airways, down to the trachea and finally is transferred to the alveoli in the lungs. The aim is to keep the alveoli and airways open and prevent their collapse during exhalation. It is feasible to provide non-invasive nasal CPAP starting in the delivery room. In extremely premature infants without the ability of spontaneous breathing, it is a very high risk of failure, so invasive support is recommended. The most important part of CPAP is it's settings. It is very essential to choose the right mode of airway pressure (standard, bubble CPAP [19], oscillating CPAP), the inlet of the air (diameter of nasal cannula, alternatively the mask or nasopharyngeal tube) and mainly the intensity of the pressure itself. Overly high pressures can cause excessive lung spacing, resulting in poor ventilation and carbon dioxide retention. The same performance as CPAP is achieved by HFNC method.

HFNC – heated humidified high flow nasal cannula

HFNC support system heats and humidifies the oxygen which is delivered to the patient with high flow-rate. Heat and high humidity of the air cause good tolerance of high nasal airflow rates. The gas is heated and humidified in a cartridge with the special membrane permeable to water vapour. This principle ensures the separation of air from water. HFNC works at various levels with flow rate 4-8 litres per minute.

Its goal is to initiate spontaneous breathing using the creation of positive distending airway pressure and reduction of lung dead space. The oxygen is delivered to the infants' body via nasal cannula. Consequently, the oxygen generates in the upper respiratory tract continuous distending pressure. However, such a pressure is not measured at all, and its value is only estimated. Some professionals are very sceptical about this device because no security valve or pressure measuring is implemented [20].

2 Methods of airway imaging

Imaging of the respiratory system is one of the many ways of its' examination. One of the most frequently performed examination in neonatal intensive care is chest radiograph (see Fig 2.1). Chest radiograph represents an essential tool in the diagnosis of pulmonary diseases. This examination is performed in case of suspected: IRDS, BPD, pneumonia, etc. Based on created radiographs, lung volumes, the shape of the lungs, lung transparency and bone structure are especially examined. In preterm infants, the chest x-ray also allows the evaluation of nasogastric probes, endotracheal tubes and arterial and venous umbilical catheters positioning. The examination is in the lying position of the infant, and the anterior-posterior projection is taken. Acquiring motion-free images of fine pulmonary structures at desired lung volumes is much more difficult in infants than in adults [21].

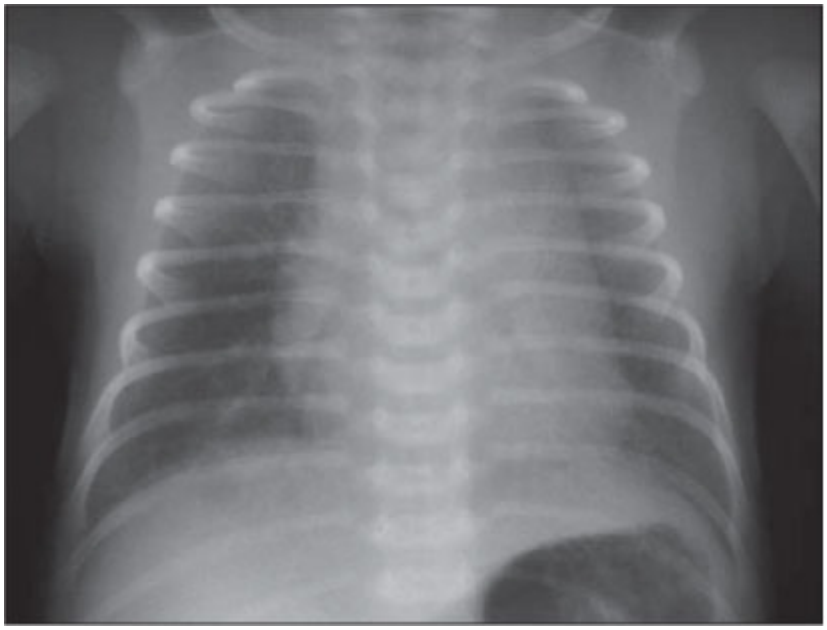

Fig. 2.1: Physiologic chest radiograph of a two-hour-old infant [21].

Subsequently, there are two standardly used imaging modalities convenient for airway examination in 3D: X-ray CT and Magnetic Resonance imaging. Each of the mentioned modalities is suitable for imaging of the distinct structures. These modalities are described in the following sections. In addition to the imaging, a physical examination is also performed. The simplest, but very useful is an observation of the general appearance of the infant and auscultation of its' breathing sound and pattern. It usually evaluated: the number of breaths, rhythm and breath depth, apnea pauses, the involvement of auxiliary respiratory muscles and presence of sonic

phenomena. Besides imaging methods and physical examination, laboratory tests are carried out under the diagnosis. These tests are performed to detect possible pathologies of the airway system. There are many types of laboratory tests. The most commonly utilized: microbiological test, complete blood count, biochemical examination and immunological examination. Lung function test is not possible to perform in infants; it is performed in kids older six years of age.

2.1 X–ray computed tomography

X-ray CT is an imaging modality suitable for investigation of the inner structure of objects. This method utilizes the X-ray beam that penetrates the patient body (in medical imaging) and the attenuation of the X-ray beam is detected (scheme in figure 2.2). The value of attenuation is given by a density of individual tissues in the patient body. Therefore it gives a non-invasive representation of internal organs and tissues. The fundamental principle of obtaining final dataset is a measurement of many projections in various angles. These measured projections are then reconstructed as a series of cross-sections through the patient body. Computed tomography is in healthcare used for both bone imaging and soft tissue imaging such as the lungs, kidneys, brain, muscles, etc. The spatial resolution of medical CT images is down to 0.2 millimetres in medical systems. In general, the higher spatial resolution of acquired images results in higher radiation doses. For a more detailed description of X-ray computed tomography imaging, see [22].

Compared with chest radiograph, using CT for detecting lung pathologies is more sensitive. CT scan is requested to confirm the presence of suspected pathology when the chest radiograph is abnormal, or some suspicion is occult due to summation projection [24]. Especially in the case of lung imaging High-Resolution Computed Tomography (HRCT) has been introduced in the 1980s. It is a computed tomography with high spatial and contrast resolution. High image resolution is made possible by the large contrast difference between the lung structures and the gas surrounding them. This implies a major requirement that the lungs should be scanned inflated. The HRCT cut thickness is usually 0.5 mm, with specialized low-dose protocols with 1.25 mm. Finer structures can be resolved with thinner slices but at the cost of increased image noise. The noise can be suppressed by the use of higher radiation dose. However, the purpose is to incur the lowest radiation dose necessary to acquire images of sufficient quality for diagnostic purposes according to the ALARA (As Low As Reasonably Achievable) principle. HRCT does not scan the whole lung volume, but only subsequent cross-sections, which are not interpolated. Thus noncontiguous acquisition technique which significantly reduces the radiation dose, can be utilized. By using HRCT, the lung tissues are not so

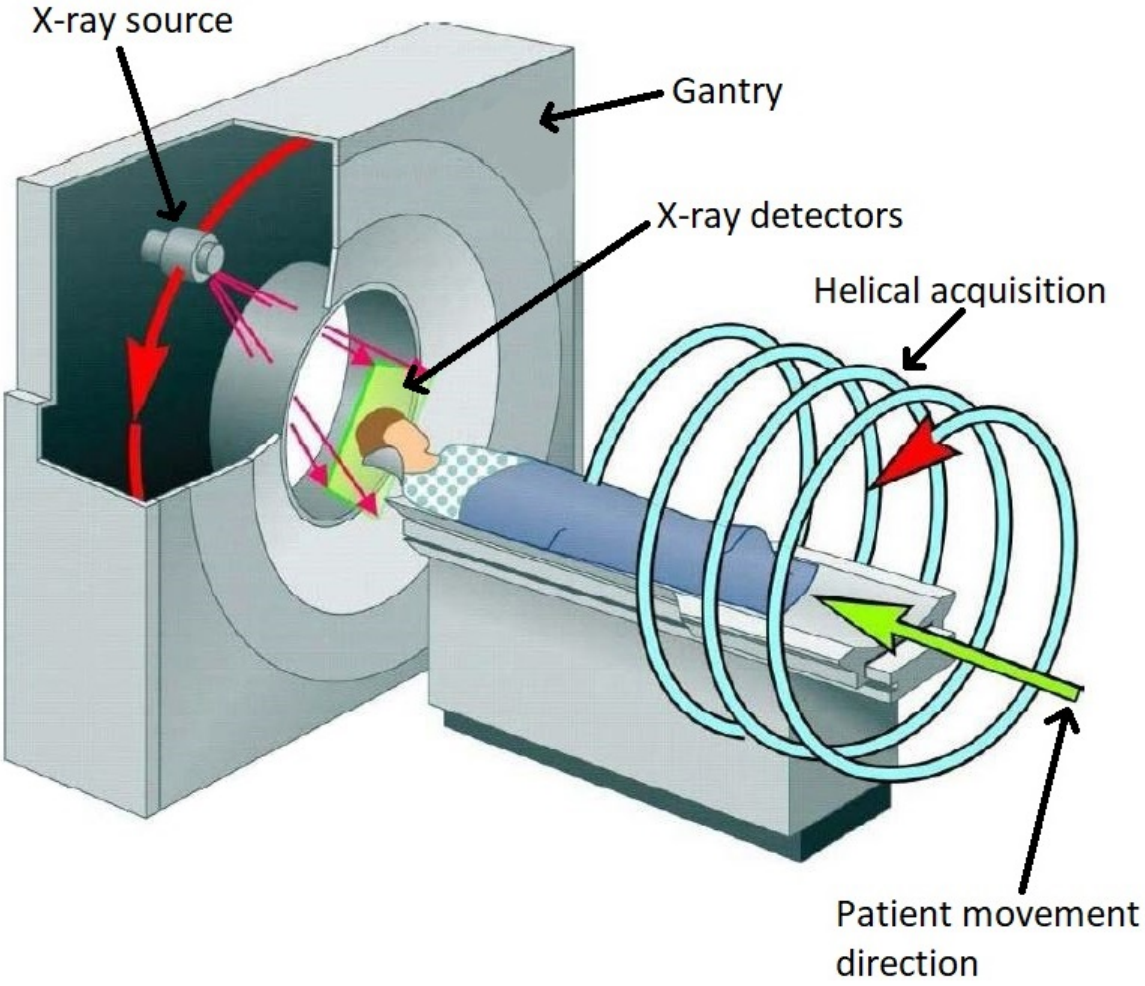

Fig. 2.2: Scheme of x-ray CT scanner and patient data acquisition [23].

blurred and the airways and vascular system are sharper than using conventional chest CT. HRCT images of the lungs are often reconstructed twice. Firstly with standard "lung" reconstruction algorithm, where is clearly visible lung parenchyma. Further, they are reconstructed with "bone" reconstruction algorithm, due to edge enhancement effects for better analysis of airways and vascular system.

Obtaining high-quality CT images of the infants lungs is very difficult due to the small size of the anatomic structures, the rapid lungs movement, and the inability of infants to hold the breath or refrain from moving. Technological advances in CT scanner speed have reduced motion artefact and allowed more infants to be scanned without sedation [24]. However, CT scanners are still not fast enough to acquire motion-free images of spontaneously breathing infants. These artifacts can be su-

pressed by transient respiratory pauses. It is no problem in sedated and intubated infant to set transient breathing pause at ventilation support system during the scan. In sedated infants with non-invasive breathing support, the transient breathing pauses are induced by synchronously applying positive pressure with face-mask ventilation to several consecutive spontaneous tidal inspirations.

2.2 Magnetic resonance imaging

Magnetic resonance is imaging technique used in healthcare for observation of anatomical structures, especially soft tissues. For imaging, MRI uses a strong magnetic field and high–frequency electromagnetic waves. The most important advantage is the absence of ionizing radiation. To date, essentially no negative effects on the human body have been demonstrated. This attribute of MRI is important especially for children who are more sensitive to ionizing radiation than adults. It follows that this type of imaging allows frequent scanning for long-term studies of chronic diseases, such as BPD. Moreover, MRI allows assessment of functional aspects of the observed tissue. The basis of the method (fMRI) is a change in blood circulation and blood volume in the investigated area. In case of chest investigation, there can be observed aspects, such as lung perfusion and ventilation, or airways and diaphragm mechanics [25]. The most common contraindications of MRI screening include: metallic implants, an allergy to the administered contrast agent or claustrophobia.

The chest MRI is challenging, especially neonatal. Imaging of chest in adult human is demanding because of the magnetic heterogeneous environment in the chest region and reduced signal-to-noise ratio due to low proton density of lung parenchyma. In the case of neonatal imaging, there is also the fact that infants have higher cardiac and respiratory rates giving motion blurring. The acquisition time is in contrast to CT very long, so there is no possibility to scan patients with hold breath or with regulated breath pulses. Thus acquisition is performed in free-breathing, non-sedated infants and the resulting images are reconstructed retrospectively in individual time-lapses avoiding motion blur. Reconstructed images approach spatial resolution that is achievable with CT, thus CT is still often preferred to MRI for chest paediatric imaging [26].

In MRI of neonates is the most common a brain development observation, respective a MRI of head. In this type of scan is visible also upper respiratory tract. The upper respiratory tract of infants has almost identical structure, thus based on head MRI scan is possible to detect sinuses or other structural abnormalities. Chest MRI is mainly demanded due to observation of lung parenchyma. Lung abnormalities, such as pneumonia or BPD usually cause increased signal intensities. MRI can

even in case of infants provide functional information regarding lung perfusion using gadolinium contrast, lung mechanics using dynamic acquisitions, and ventilation using inhaled hyper-polarized gases [26].

Recently, there is an ongoing research of neonatal MRI scanner. This scanner is designed specially for infants, who can be scanned directly in the neonatal unit, see Fig.: 2.3. Unfortunately, this scanner is still not used in clinical practise [27].

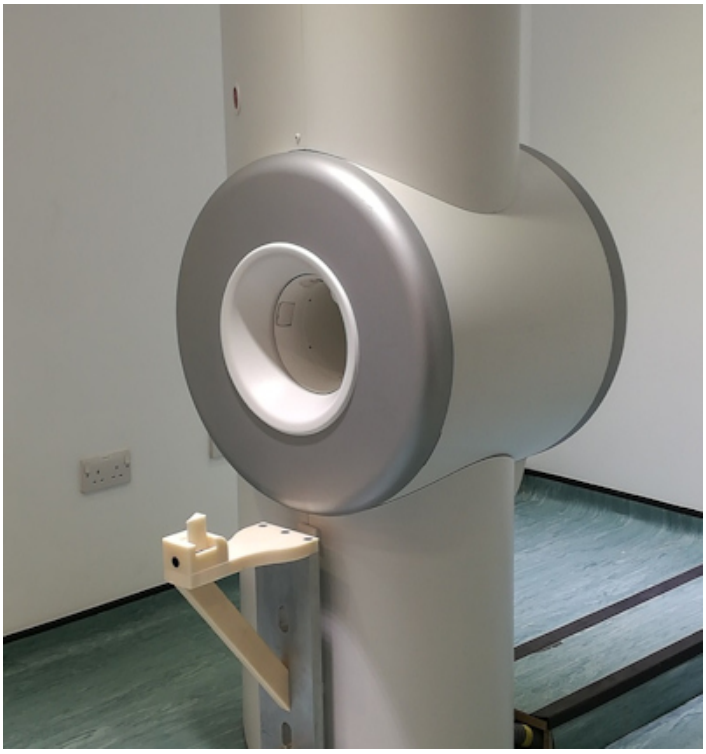

Fig. 2.3: Neonatal MRI scanner developed by GE company [27].

3 Formation and application of pulmonary models

Pulmonary models have been developed to understand the physical properties of human airways. These models serve for CFD (Computational Fluid Dynamics) analysis or particle deposition measurement. Physical measurements in pulmonary models allow deeper insight into internal flow dynamics of the respiratory system. There are multiple ways of obtaining respiratory tract geometry. Before the arrival of modern imaging methods, the geometries were obtained as wax castings from corpses. This in-vitro approach is based on filling the airways of corpse body with wax or resin, which then solidifies. Solidified material is then removed from the body. For further digitization can be this material using a 3D scanner or CT converted to data form [28, 29]. This approach is still utilized in geometry preparation. The main advantage is the possibility of high spatial and contrast resolution of scanning. However, the injection of airways with the wax or resin is complicated and can cause inaccuracies in geometry due to incomplete filling.

The conventional way of producing airway geometry is based on airway acquisition with HRCT. The scans are obtained with nearly full inspiratory volume due to better air/tissue contrast. In the case of physiological model creation, the patient must have lungs free of pathological alterations. The airway geometry itself is based on the airway segmentation. Airway segmentation approaches are described in chapter 4.1. The segmented model is afterwards exported in the form of a polygonal triangular network describing the geometry of the airway surface. The suitable standard format for work with vector models is (Standard Tessellation Language) STL. *.STL* files describe only the surface geometry of three-dimensional objects and are therefore suitable for working with tubular models. The conversion to surface representation is followed by model smoothing and removal of isolated components.

Within the model development, the emphasis is placed on its accuracy. On the other hand, there is often a demand for model simplification. This simplification eases evaluation of further analysis and reduces computational time. The accuracy of the obtained results is compromised, but the model can still provide representative estimations of evaluative parameters. Simplification of the model is based on approximation of individual parts with simple geometric shapes. In case of airways, models are used cylinders approximating individual pulmonary pathways. The final accuracy depends on the correctness of pathways approximation, especially on selected branching angles and branches dimensions.

Anatomically-accurate adult models based on HRCT measurement are generally limited to the first 6 or 7 generations due to imaging resolution [30]. The digital

models are utilized for numerical modelling and simulations. To validate these results, the model can be manufactured and subjected to physical testing. The geometry production is possible by any suitable rapid prototyping technique. The most suitable technique for model printing is currently stereolithography.

3.1 Characterisation of airway models

Airway models are usually developed for evaluating some desired parameters. These parameters, in case of airway models, are in general air-flow measurement and particle transport and deposition. For example, research on drug delivery or sleep-related respiratory disorders is being conducted based on knowledge of these physical attributes in the human respiratory system. In the case of prematurely born babies, airway model can help to improved administration of respiratory support. The knowledge of actual pressure and velocity fields within the respiratory system can consequently lead to improved administration of respiratory support to newborns in need. The process of airway model evaluation is usually divided into two sections:

1. Numerical simulations
2. Validation of simulated data

An evaluation may vary depending on the purpose of the model. Most common measurements consist of: Aerosol flow simulation, micro and nanoparticles deposition, measurement of liquid aerosol velocities and deposition and study of turbulent modelling methods.

3.1.1 Numerical simulations

There are two main approaches developed for numerical simulations: Analytical (stochastic) model and numerical model. Both simulations describe particle trajectories and its deposition in the airway model. The geometry for the analytical model has to be strongly simplified and analytical equations describing the model have to be derived. Therefore the numerical model is often utilized. These models are based on computational fluid dynamics (CFD) and allow to compute desired particle attributes by numerical algorithms even in realistic 3D airway geometries.

In order to obtain an accurate simulation, setting the initial breathing conditions is crucial. As a breathing pattern is usually proffered sinusoidal course which represents physiological conditions. Next parameters are variable. Tidal volume in adults ranges in 350–600 ml. In preterm infants is computed as 4-6 ml/kg of body weight. Respiratory cycle depends on many circumstances, in adults is about 12-15 breaths per minute which correspond to 4-5 seconds per one cycle. In infants generally is

respiratory rate 30-40 breaths per minute which correspond to 1.5-2 seconds per one cycle. The inspiration/expiration ratio is approximate of 1:2 [31].

3.1.2 Validation of the computational model

The first step of the validation is to create an experimental setup. The airway model based on real airway geometry is possible to produce by rapid prototyping techniques. The material of the model should imitate the attributes of human airways as best as possible. For this reason is inner surface often coated with a surfactant-like substance to ensure real behaviour of inflowing particles.

During the experiment is inside the model inflow aerosol containing various particles. The size of the particles depends on the purpose of the study, but the size has to correlate with the validated numerical simulation (if available). Frequently particles with a diameter ranging from 0.1 to 10.0 micrometres are utilized. The particle generator create realistic conditions of aerosol (temperature, humidity, etc.).

There are many methods suitable for aerosol flow measurement. The aerosol velocity and deposition can be measured by traditional methods requiring liquid aerosols. One of them is a hot wire anemometry. Hot wire anemometry is an invasive technique when a probe is inserted to the model. The technique is accurate but disrupts the aerosol flow. Another traditional method is non-invasive optical measurement using laser Doppler anemometry. This method requires very high optical purity of the model material but is able to determine the characteristics of turbulent particle transport in human airways under steady and cyclic flows [32].

Recently, there are available medical imaging scanners capable of measuring the aerosol flow or deposition in the airway model. When the radionuclide is bound to the carrier microparticles, the deposition of the aerosol can be observed by Single-Photon Emission Computed Tomography or Positron Emission Tomography. The evaluation of aerosol deposition in individual segments of the model is based on a volume radioactivity analysis [33].

The velocimetry of aerosol is possible to measure by Magnetic Resonance Gas Velocimetry Aerosol flow velocities are usually obtained by phase–contrast imaging. The measurement can be applied using conventional medical MRI scanners, but in case of aerosol are often no hydrogen protons to detect, so another detectable element or liquid aerosol has to be chosen [31].

4 Image processing

Image processing is a set of methods that perform some mathematical operations on a multidimensional signal – image. These operations are executed in order to get an enhanced image or to extract some desired information from it. The image can be N-dimensional, the standard volumetric image is represented as a function *f(x,y,z)* which determines a brightness intensity of the pixel at coordinates *x,y,z*. The output of image processing operation may also be an image or required features associated with that image. These features may be intensity values of individual parts of the image, dimensions or volume of a selected area in the image, etc. For the majority of analyses, the image needs to be pre-processed and then segmented.

Preprocessing often enhances some image features essential for further processing and increase the accuracy of the segmentation. The individual preprocessing steps are selected according to how the input data is affected. These steps often consist of image normalization, sharpening, denoising or transformation. In standard airway analysis procedure after preprocessing follows segmentation of these airways.

4.1 Airway segmentation

Image segmentation is a process that divides an image into parts with mutual features. The main goal of the segmentation is to recognize the region of the interest. To each pixel in the image is assigned a label which characterizes if the pixel belongs to the region of interest or not. There may also be more of these regions in the same image, and in this case, each pixel is assigned a label which corresponds to the selected region. The result of segmentation is then again the image of the same dimensions as the original, in which the individual regions are depicted.

Based on the literature review, the upper respiratory tract is often segmented with thresholding and subsequent manual correction. Firstly VOI (Volume of Interest) of the upper airway is created [34]. All pixels in this VOI below a chosen pixel intensity are identified as air and all above as tissue. The Otsu algorithm [35] or variants are often used. The final value of the threshold depends on the used scanning modality and scanning protocol. Manual correction as post–processing is often crucial for reaching accurate airway segmentation and smoothed airway mask [36].

More sophisticated approaches for upper respiratory tract segmentation utilize active contours. Bui et al. [37] developed a multi-step segmentation algorithm based on combining a global and localized region-based active contour. At first, VOI is automatically located based on Gaussian mixture model thresholding and morphological operators. Morphological operators are applied to close the openings,

fill up the airway and remove the noise. The global active contour is initialized in the VOI. As energy for contours is used Kullback–Leibler (K–L) [38] divergence. A subsequent anisotropic localized region-based active contour is used to refine the coarse segmentation.

Next possible approach for upper respiratory tract segmentation is the utilization of fuzzy connectedness. Fuzzy connectedness is a global fuzzy relation that, based on affinity, helps determine how the voxels hang together globally in the scene to form the object. This approach is suitable for MRI data. Firstly the intensity correction and VOI containing the airway is created. Then an initial seed in the VOI must be specified. Subsequently is determined local fuzzy relation of all voxels in VOI to the selected seed voxel. This relation is based on the training area, which is denoted manually in one section in the scene. The relation indicates how the voxels hang together locally within the scene in the object of interest. The final segmentation is based on the strength of relationship of individual voxels to the object. Voxels with higher strength than a specified threshold are assigned to the airway mask. The threshold is chosen empirically, but thanks to prior intensity correction, this approach works for all datasets obtained with the same scanning protocol. For a more detailed description of this approach, see [39].

The fundamental algorithm for lower airway segmentation is generally the method of region growing in 3D space and its modifications. However, there are many other segmentation approaches, and the suitability of their use differs, especially in the quality of measured data, where the determinative factor is a contrast between the airways and the surrounding tissues. The contrast is in particular given by used imaging modality and by the size of airways which is relatively tiny by infants.

The basic variant of segmentation by this method represents segmentation using the selected static threshold. This method is effective only in places where the internal bronchial radius is approximately 5mm. In case of premature infants, this diameter approximately corresponds to newborns trachea [40]. For smaller diameter bronchi, the bronchial wall is very thin, and therefore the edge representing the transition from bronchus to surrounding tissues is less contrasting and cannot be detected by a static threshold [41]. Due to insufficient contrast between the air and bronchial wall is used a dynamic threshold, where the actual threshold value for individual initial seeds is calculated based on the surrounding pixels. Thanks to this modification the segmentation is possible down to the bronchi of 3mm diameter. Next possible modification of region growing algorithm for better segmentation results is the eliminating leakage of expanding segment outside the airways. If leakage of an emerging segment is detected in one part, the segmentation algorithm can be stopped only in this leaking part, and the segmentation can continue in the other parts of the pulmonary tree. Leaks are characterized by a narrow bottleneck

connection to the seed area and by a dynamic change of average pixel intensities outside the airways. In addition, segment leakage can be controlled by approximate knowledge of the shape and internal diameter of the airways in each part of the pulmonary tree [42].

Many recently published methods utilize convolutional neural networks for segmentation of airways. These approaches often deal only with bronchial tree segmentation by adult patients. The conventional way for images segmentation is the utilization of a series of 2D images. Authors in [43] proposed a segmentation method based on creation patches through the airways with the use of information from all three orthogonal directions (axial, sagittal, and coronal). A patch group in each direction is passed through one of three separate identical stacks of CNN. These three parallel stacks are combined into the first fully connected layer. This architecture is called 2.5 dimensional CNN because of the use of two-dimensional images contain constrained three-dimensional information.

In the case of whole airways (upper + lower) segmentation, there is a problem with data acquisition. Usually, the patient's head for upper and chest for lower airways are not scanned at the same time with one acquisition protocol. For obtaining whole airways is often needed to combine multiple datasets. Utilization of CNN for whole airways segmentation in data of premature born babies scans would have to be split into 2 phases. In one phase the upper airways would be segmented and in the second lower airways. Other segmentation approaches can utilize at first combination of datasets and then airway segmentation. Additionally, there is no public dataset of training data containing newborns airways.

Generally, for airway segmentation, MRI data offers the best air/tissue contrast, but movement artefacts can occur due to the long image acquisition time. Other difficulties can often cause a non-isotropic voxel size. In CT data, there are limited movement artefacts, due to the short duration of the scan. Spatial and contrast resolution is suitable for airway segmentation, but this type of data suffers from poor soft tissue differentiation, and streak and beam-hardening artefacts [36], see Fig.: 4.1. All these methods mentioned above were designed at adult patients, where the airways have greater diameters than at infants, and the transition between air and tissue is sharper than at infants.

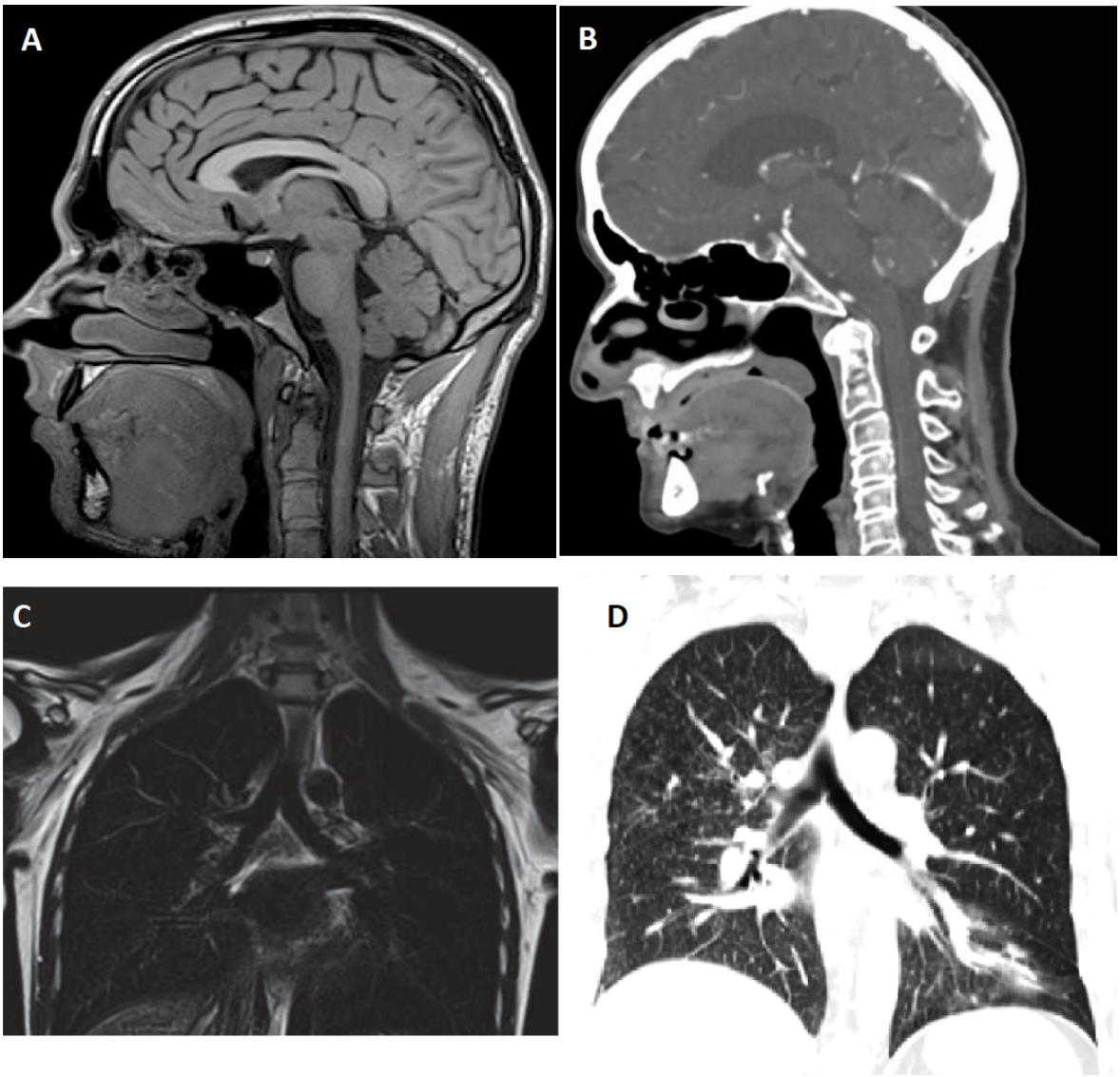

Fig. 4.1: (A) T1 weighted MRI image of brain – all upper airways are clearly visible, (B) CT scan, brain scanning protocol – all upper airways are clearly visible with possibility of threshold segmentation, (C) T2 weighted MRI image of lungs – airway tree is visible only down to second branching generation, (D) CT scan of lungs with vascular contrast agent, lung scanning protocol – more generation of airway tree is visible than in part (C).

4.2 Evaluation of segmentation quality

The quality of image segmentation can be evaluated objectively. In general, objective evaluation is based on the comparison of the evaluated and the reference image. The result of segmentation quality can be interpreted differently according to the chosen evaluation metrics. There are more types of these metrics. Most of them are based on the computation of spatial overlap accuracy. The overlap is often computed according to these statistical indicators. True positive – the proportion of actual positive pixels that were correctly identified in the object according to the reference. True negative – the number of pixels that were correctly identified as not belonging to the segmented object. False positive – the number of pixels that were incorrectly identified as part of the segmented object. False negative – the number of pixels that were incorrectly identified as not belonging to the segmented object.

Dice coefficient

Sørensen - Dice, in short, Dice coefficient, is used to determine the general similarity of two samples. This coefficient in image-processing is often applied to segmentation quality evaluation, especially due to the easy interpretation. The range of Dice coefficient is from 0 to 1. The maximum value indicates the absolute overlap of the two segmentation masks. The value of 0 indicates no overlap [44]. The coefficient is calculated according to equation 4.1.

$$DSC = \frac{2TP}{2TP + FP + FN} \tag{4.1}$$

Jaccard

The Jaccard coefficient is not very different in form from the Dice coefficient. This the metric is also used to determine the similarity and difference of two sets of samples. In contrast to the Dice coefficient, Jaccard considers both segmented masks as independent samples. Thus, the segmentation quality is evaluated more strictly because the true positive is not multiplied by 2 (see equation 4.2).

$$JSC = \frac{TP}{TP + FP + FN} \tag{4.2}$$

5 Creation of infant airway model

For a description of a representative airway model, it is necessary to avoid any radiographic artefacts and pathological conditions present by measured infants. These imperfections may lead to the wrong anatomical shape of the resulting model. To avoid this error, the proposed representative model is based on three particular airway models. The number of three models is precise enough to create a representative model. However, it is not possible to achieve a normal distribution of the evaluated parameters of particular models. Therefore, the representative model can only be related to these three particular models, but not to the whole population. The number of three particular models creation is given by all available data to this study.

The intersubject variability of the upper airways of infants is not very significant since they do not have pharyngeal tonsil and nasal cavities. The shape is mainly pronounced by the paranasal sinuses and adenoids which are not present at infants' age. The upper airways take its variability mainly during the first years of life [45].

The variability of lower airways manifests primarily in higher generations of branching of the bronchial tree. The diameters of higher generations of bronchi are similar, but their number and length may vary. However, this variability of the respiratory tract is negligible in the creation of a representative model, due to the description of this model based on the primary bronchi evaluation.

The advantage of the approximately uniform shape of neonatal airways lies in the fact that the final representative model can be represented as an average of more particular models.

5.1 Obtained data

In this study, sufficient amount of datasets were available to create three particular models. Every model is based on two diagnostic measurements. The first one is always an MRI scan of the head of 2 weeks old patient born in 30^{th} week of gestation. The second scan is CT of lungs with the one-month-old infant with an unknown week of gestational age, but surely premature. These CT datasets were chosen from all available datasets due to the best dimensional similarity to fundamental MRI head scans. The parameter for similarity evaluation was trachea diameter. The diameter was evaluated in the three selected trachea cross-sections, and the most similar dataset was chosen. Proposed dataset combination is necessary, because no dataset containing both – upper and lower airways, was available to this study. Based on the fundamental MRI scan of upper airways, all of these created models correspond to the airways of an infant born at the age of 30 weeks of gestation and scanned

two weeks after birth. The available data are collected from several child-hospitals world-wide. All of them were obtained in their original unchanged form in DICOM format. For acquisition parameters, see table 5.1.

Tab. 5.1: Data acquisition parameters:

Original data		
	MRI	X-ray CT
Bit Depth	16	16
Resolution [px]	320 × 320 × 144	512 × 512 × 78
Voxel size [mm]	0,5 × 0,5 × 2,5	0,34 × 0,34 × 1,25
Data after resampling		
	MRI	X-ray CT
Bit Depth	16	16
Resolution (approx.) [px]	620 × 600 × 1600	820 × 800 × 485
Voxel size [mm]	0,2 × 0,2 × 0,2	0,2 × 0,2 × 0,2

5.2 Proposed algorithm

The proposed algorithm runs in several steps. There are two inputs to the algorithm corresponding to two image datasets described in chapter 5.1. The output of the algorithm is a particular airway model, which is consequently evaluated by the evaluative algorithm described in chapter 6. The major task for particular model creation is model segmentation. Segmentation is a two-steps process based on pre-processed data. At first, the majority of segmented air in the airways is segmented by the automatic region growing approach. Consequently is this segmented mask adjusted by fine manual segmentation. The segmentation masks are consequently registered to obtain the particular airway model. All three particular models are consequently evaluated to describe the parameters of the representative model. The whole process is depicted in Fig.: 5.1 as a block diagram. A more detailed explanation of the algorithm is described in the following sections.

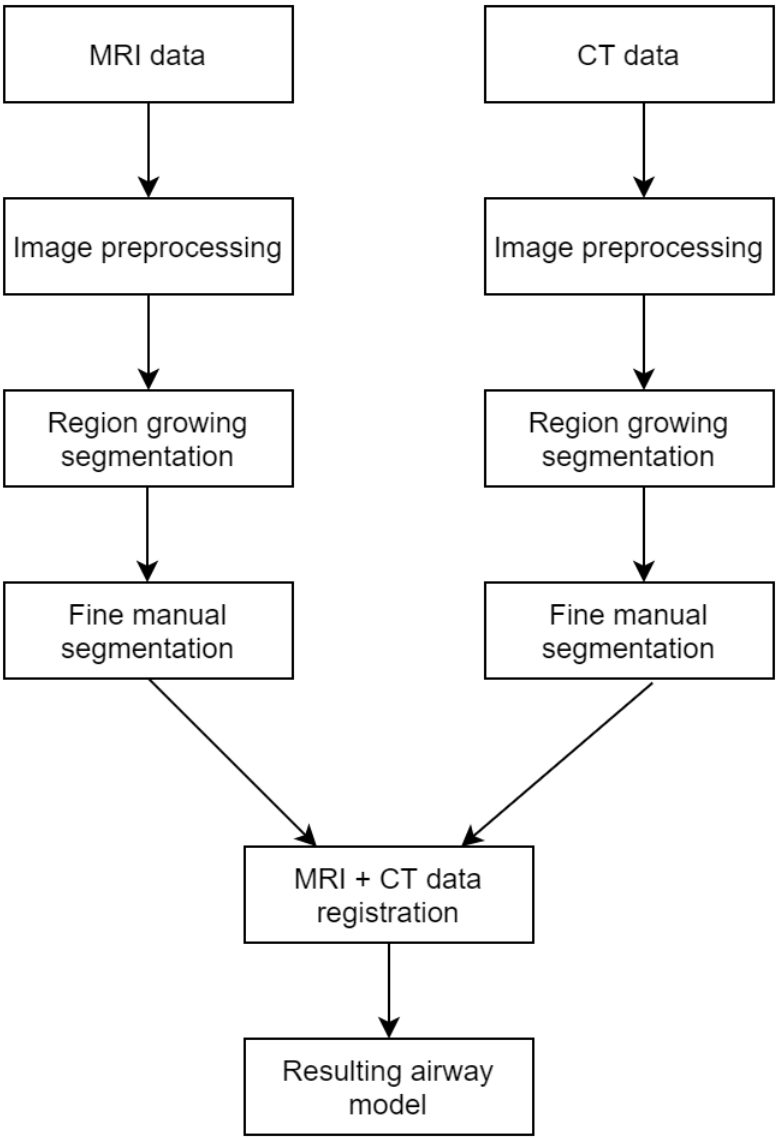

Fig. 5.1: Block diagram of the proposed algorithm

5.2.1 Image pre-processing

Image pre-processing consists of image resampling, cropping and image filtering. At first, image dataset is converted to double data type. Image resampling is executed to achieve isotropic voxel resolution. As an output of this image interpolation was empirically chosen voxel size of 0.2 mm. This voxel size is the best compromise, between stair-step artifact reduction and reasonable size of the image volume.

Datasets were interpolated in all three dimensions to obtain identical voxel dimensions as in X, Y and Z plane. For image interpolation was utilized cubic interpolation method. The cubic interpolation method is standard resampling method in

image-processing, which in general produces smoother images with less resampling artifacts than other resampling methods.

The second step of image pre-processing is image filtering. Based on [46] was chosen bilateral filter for image enhancement. The bilateral filter is nonlinear and is used for image smoothing and noise reduction while preserving edges. The kernel of filtration here depends not only on the distance but also on the intensity of the surrounding pixels to the investigated pixel, see Equation 5.1.

$$BF[I]_p = \frac{1}{W_p} \sum_{q \in S}^{\infty} G_{\sigma_S}(\| p - q \|) G_{\sigma_r}(I_p - I_q) I_q \tag{5.1}$$

Where W_p is a normalization factor, G_{σ_S} is a spatial Gaussian that decreases the influence of distant pixels. G_{σ_r} is a range Gaussian that decreases the influence of pixels q with an intensity value different from Ip. Only pixels close in space and range are considered in the computation of the central pixel p. More about bilateral filtering, see [47]. In this case, for filtering was chosen Gaussian kernel with standard deviation = 3 and size of the filter = 5 voxels. These parameters were obtained heuristically, according to results of further automatic segmentation. Results of the Bilateral filtering are depicted in the Fig.: 5.2.

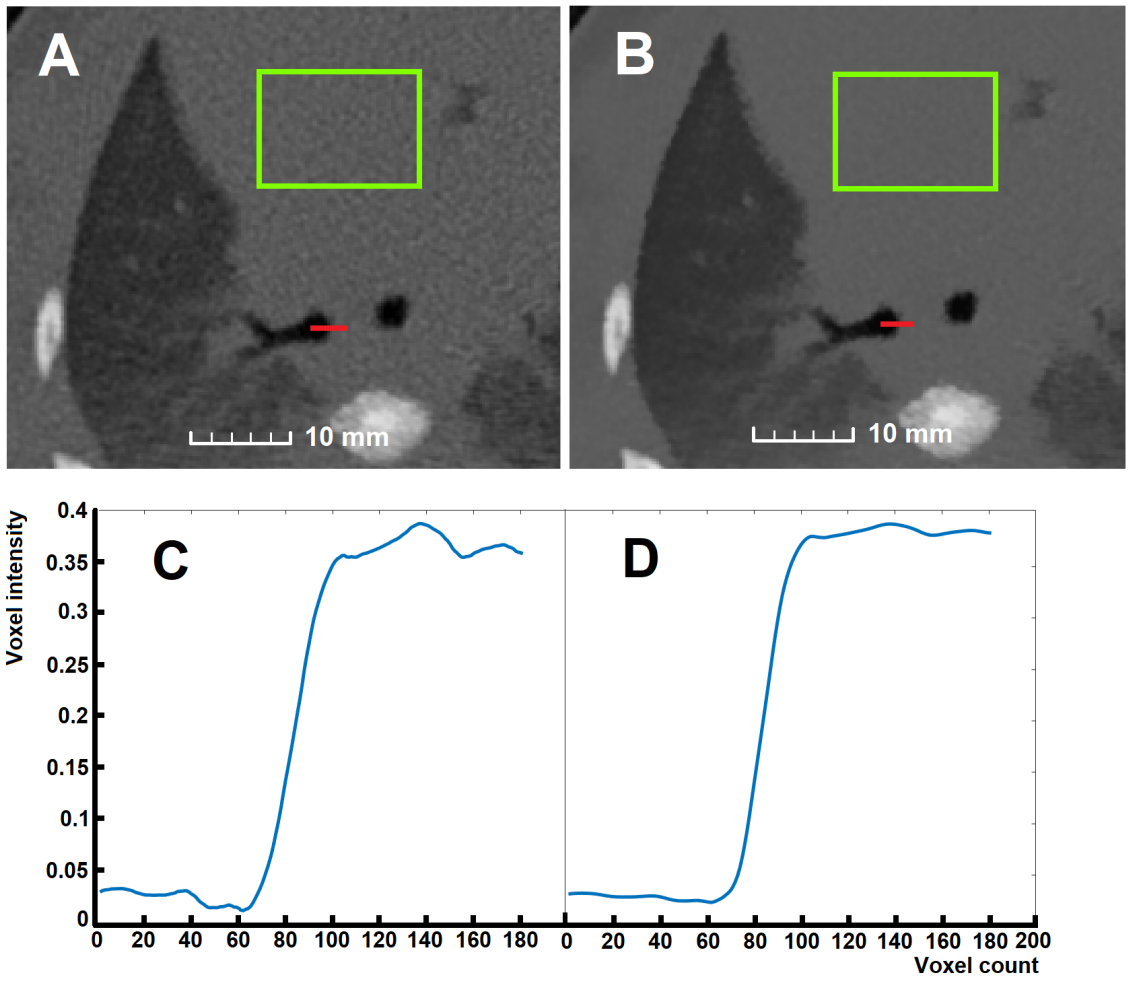

Fig. 5.2: Impact of bilateral filtering. (A) Original image, (B) Result of bilateral filtration. Green rectangles mark the area for standard deviation calculation. Red lines mark the area for line profiles depiction. (C) Line profile of original image, (D) Line profile of filtered image

According to Figure 5.2, the degree of smoothing by the bilateral filter was evaluated. For this purpose, the standard deviation and line profile were calculated. Standard deviation in original and filtered images was calculated in the area marked by the green rectangle. The location of line profile calculation is depicted by a red line in both images. The standard deviation in the original image: 0.0027, in the filtered image:0.0015. The standard deviation is confirmed by the line profiles in sections C and D. In the line profiles images is visible, that the image after bilateral filtration is smoother compared to the original image.

5.2.2 Image segmentation

Segmentation of both image datasets is based on custom-written Region Growing algorithm. The algorithm itself is automatic and was developed in Matlab programming environment. There are two inputs: 1) Volume of images (MRI/CT), 2) Threshold value for segmentation. This threshold value corresponds to the maximal mean value in 26-connectivity to considered voxel. The initial seed position is determined automatically. This position is found as minimal pixel intensity in the image (corresponding to segmented air) surrounded by 10x10x10 voxels with similar intensities. In MRI data of upper airways is this initial seed determined in the nasal cavity. In CT data of lower airways is an initial seed selected in the trachea, which is the standard location for initial seed placement in case of lower airways segmentation. This automatic determination initial seed method works robustly for utilized datasets.

The decision, about adding the considered pixel to the growing segment, is based on the threshold value. The threshold value is computed as a mean of values in 26-connectivity mask surrounding the considered pixel. If the considered pixel is added to the growing segment, its' 6-connected neighbourhood is automatically considered as initial seeds. The algorithm aims is to segment an air contained in the airways. The growing segment proceeds through the airways until it encounters a tissue or (developing) bone. In that case, the voxel under consideration is added to the segment, but its 6-connected neighbourhood is no longer added to the iteration cycle, so the segment will no longer grow in that direction.

In the case of upper airways segmentation, the proposed algorithm works correctly in the nasal cavity. At the site of the nasopharynx is air/tissue contrast very low, additionally are these cavities very narrow by infants, so there the growing segment stopped. These locations were additionally segmented by fine manual segmentation. In case of lower airways worked this algorithm properly up to the second generation of branching. Additional bronchi were also segmented by fine manual segmentation. In this way, it was possible to segment the bronchi for a maximum of the fourth generation of branching. For results of segmentation, see Fig.: 5.3.

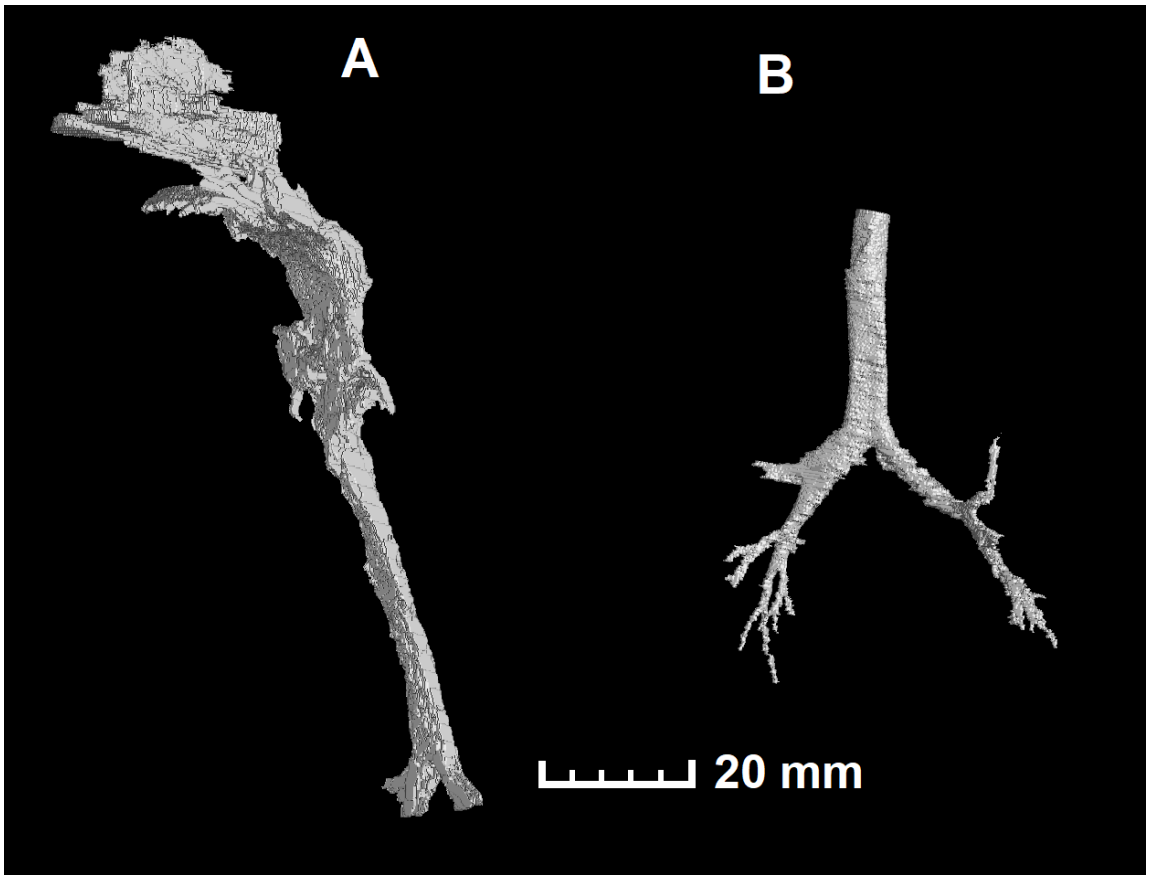

Fig. 5.3: Resulting segmentation. (A) Upper airways, (B) Lower airways

5.2.3 Image registration

The output of the segmentation part of the algorithm is always two masks corresponding to the upper and lower airways. These two masks have to be registered, to create one unitary airway model.

Image registration algorithm works semi-automatically. At first, automatic pre-alignment takes place. This step facilitates further manual final registration. The pre-alignment step works in three main steps. At first, both datasets arrays are padded with zero-values, to get the same dimensions of these arrays. Consequently are detected centroids of both volumes. The detection is based on the analysis of the connected components, which is already implemented in the programming environment [48]. The centroid of the whole volume is consequently shifted along the z-axis, based on the ratio between the whole volume and the principal axis length. In this manner, approximately the middle of the trachea is found. Subsequently, the relative magnitude of the displacement between both centroids is calculated. Based on the direction and magnitude of the shift, the upper airway MRI data is shifted

so that the centroids of both datasets overlap (see Fig. 5.4).

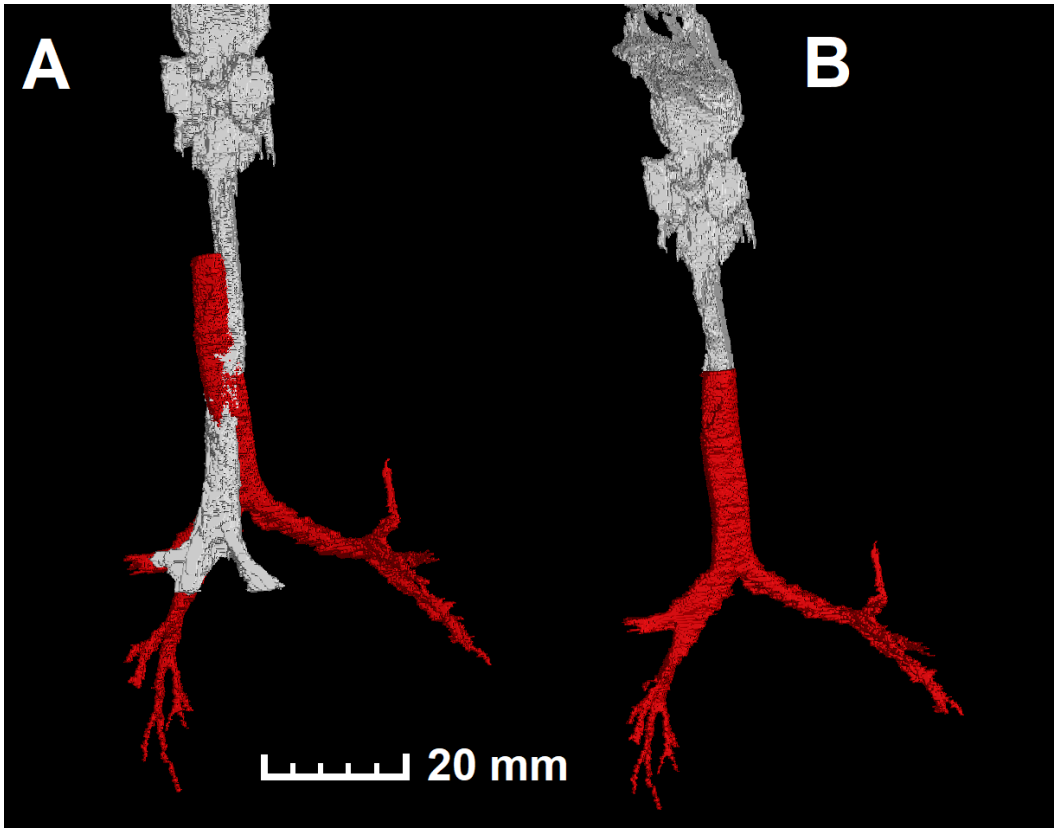

Fig. 5.4: Image registration process (A): Result of the image pre-alignment (B): Resulting model, trachea is preserved from lower airways dataset (red colour)

Manual registration is executed in software Avizo, the product of Thermo Fisher Scientific. The main task is to shift and rotate segmented lower respiratory tract data to overlap the trachea volume as much as possible. The resulting relative position of the trachea from the upper and lower airways is found based on the primary bronchi branching. The tilt of the lower airways was adjusted to ensure maximum tracheal overlap in both masks.

The overlapping part of the trachea, which is present in both datasets was preserved form CT dataset due to the higher air/tissue contrast, and thus higher relevance of trachea segmentation. The location of the tracheal connection is based on the maximal restriction of stairstep artefact. The trachea dimensions are approximately identical in both datasets so that multiple locations could be found. The final location was determined to preserve maximal part of the trachea from CT data.

5.3 Particular newborn airway model

The result of the proposed algorithm is three particular airway models. These models are corresponding to an infant born in 30^{th} week of gestation and scanned 14 days after birth. Thus, the models correspond to the 32 weeks old infants. In Fig.: 5.5 are depicted resulting models composing always of two utilized datasets. All particular models include whole airways except for the oral cavity. It is not possible to recognize the oral cavity according to spatial and contrast resolution of available datasets. The oral cavity is in case of modelling infants' airways negligible due to administration of breathing support via nasal cannulas. The description of a representative model is based on these three particular models (in Fig.: 5.5).

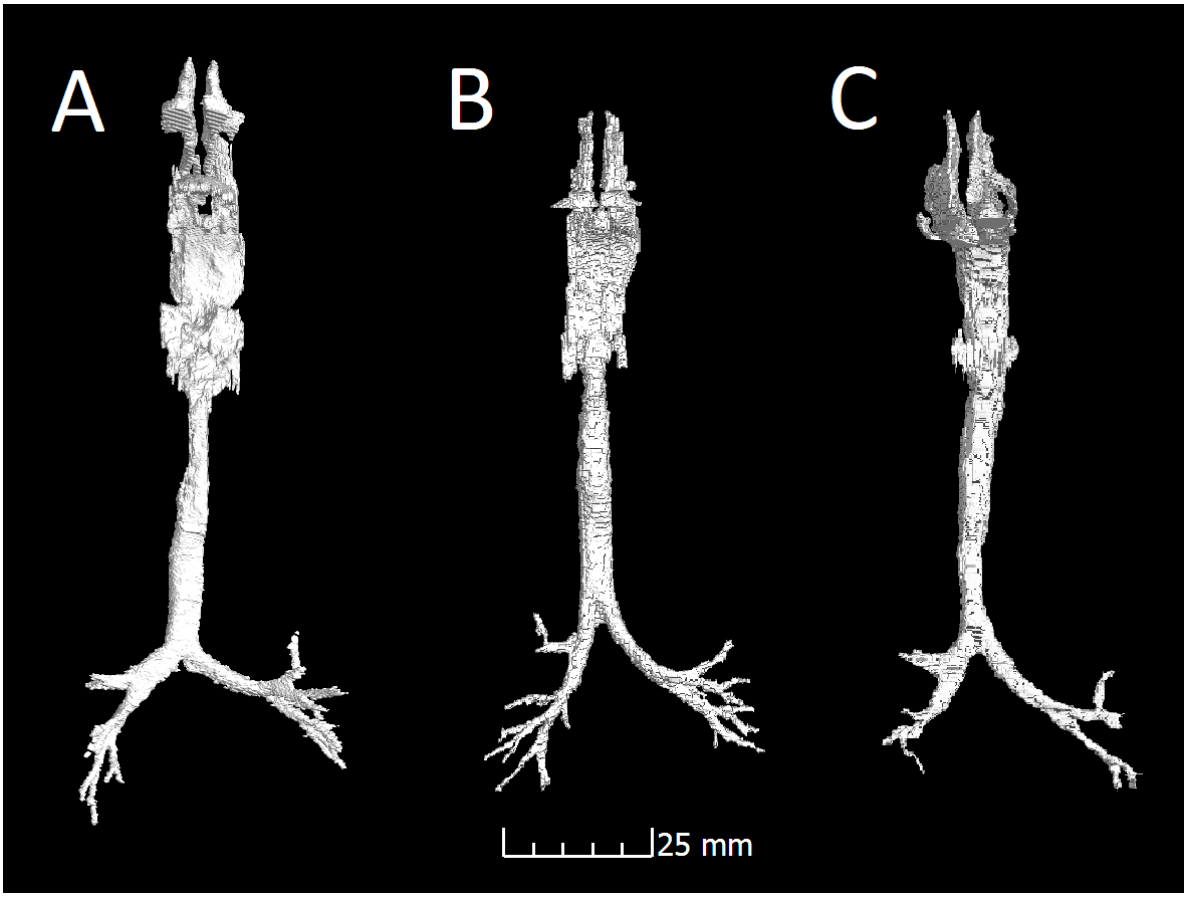

Fig. 5.5: Resulting infant airway models. (A): Model 1, (B): Model 2, (C): Model3

6 Evaluation of infant airway model

The incidence of any pathological conditions associated with lung development is related to the gestational age of the newborn. In addition to the lack of surfactant production, it can also be the anatomical development of the respiratory tract. In this thesis, several parameters were chosen to evaluate the anatomical development of the respiratory tract. Although the respiratory tract development should be in all individuals very similar in certain gestational age, analysed parameters values may vary. To evaluate these differences, all three created models were analysed individually. The resulting parameters describing the representative model were obtained by the knowledge of the means of the individual parameters from each analysed model. The methods for obtaining these parameters from each model are described in Chapter 6.1.

6.1 Evaluation of particular models

The representative model of newborn's airways is based on three created particular models. There were selected twelve parameters describing the models' anatomy. These parameters were evaluated based on a custom-written algorithm in the Matlab® programming environment.

All evaluated parameters related to the measurement of a certain length in the model are obtained on the basis of 3D image skeletonization. The skeletonization is performed using a function implemented in a programming environment that utilizes a thinning algorithm to calculate the skeleton. The skeletonization also removes very short branches where the demand for minimal branch length is three voxels. Consequently, the skeleton is converted to a network graph, based on the algorithm by Kollmannsberger [49]). This function converts a 3D binary voxel skeleton into a network graph described by nodes and edges. Each node corresponds to the start or end-point of individual skeleton links. Furthermore, bifurcations or multi-furcations are also represented by nodes. The edges between individual nodes contain the information about the position of voxels corresponding to the part of the skeleton connecting specified nodes. The graph representation is essential for the analysis of individual parts of airway models.

The network graph is cleaned from false nodes caused by segmentation and skeletonization artifacts. This step is based on the knowledge of individual branches length and nodes connectivity. If one node is not a start or end-point and connects only two branches, that node is removed, and both branches are joined.

Based on the graph representation, the model is divided into five individual Volumes of Interests (VOIs). These VOIs correspond to upper and lower airways,

trachea and left and right main bronchi (see Fig.: 6.1). Individual VOIs are utilized for volume analysis of corresponding model parts. The final volume of any VOI is calculated according to the knowledge of the number and size of the corresponding voxels. This division into VOIs is possible based on the knowledge of connectivity between individual nodes in the graph representation. The node corresponding to the trachea end-point is connected with nodes corresponding to the end-points of both main bronchi. According to the anatomical shape of the airways, it is possible to find these key points. The methodology for determining all parameters is described below.

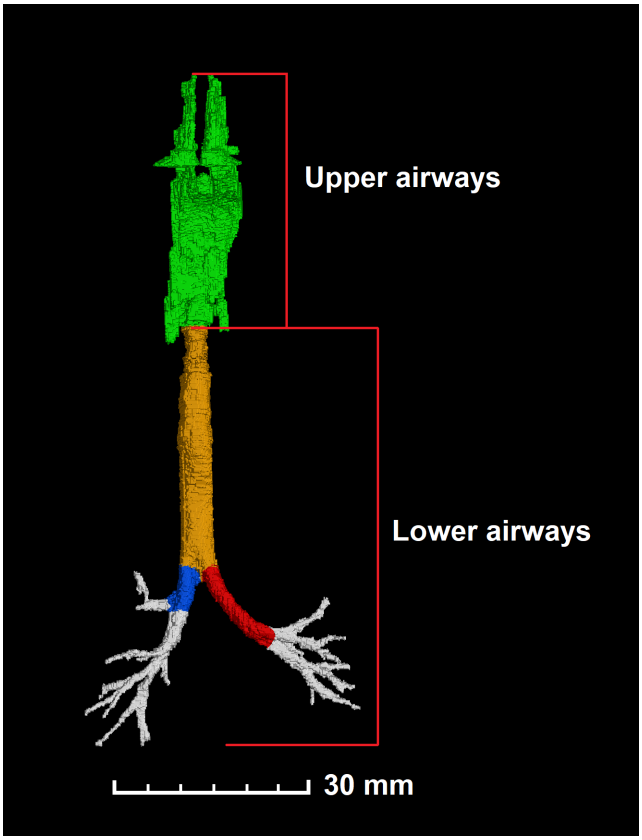

Fig. 6.1: Division of the model. Green color: upper airways, Yellow color: trachea, Blue color: right main bronchus, Red color: left main bronchus, White color: next bronchi.

Model volume

The computation of model volume utilizes all voxels corresponding to the airways (segmented mask). The total volume is computed, using the knowledge of the number and size of the voxels in the segmented mask. This volume also corresponds to the amount of air which is contained in the segmented airways.

Upper airways volume

Upper airways include the nasal cavity, nasal passages, paranasal sinuses, the pharynx, and upper part of the larynx above the vocal cords. Based on the skeleton evaluation, the vocal cords location is detected. This area is identified as multiple branches in the skeleton prior to the long line corresponding to the trachea. The VOI of upper airways is defined as all voxels from top of the model up to the vocal cords.

Lower airways volume

Lower airways include the main part of the larynx (below the vocal cords), trachea, bronchi and bronchioles. The VOI of lower airways is created in a similar manner as VOI in the upper airways - all voxels below the vocal cords up to the bottom of the model are included in this VOI.

Trachea volume

The upper location of tracheal VOI is selected in the location of transition between the larynx and trachea. The larynx is detectable thanks to the long skeleton branches. The lowest skeleton branching of the larynx followed by a long line without branching corresponds to the trachea. The end-point of the trachea is stated in the point of skeleton branching into two main bronchi. To obtain valid results, the trachea is extracted as the largest part of the analysis of the connected components in the corresponding VOI (to exclude ascending bronchioles).

Model length

Model length is calculated as the shortest path of the skeleton graph representation connecting the upper point in the model (corresponding to nasal passage) with the end of the trachea. The upper point is detected according to the graph representation properties, and the end-point of the trachea is known from the prior detection. The next step is to detect the shortest path in the graph between these selected points. This step is calculated by function already implemented in the programming environment. This function utilizes the Dijkstra algorithm to find the shortest path [50]. The final length is calculated as Euclidean distance between adjacent voxels in skeleton in the detected shortest path. This distance is normalized by voxel size to obtain the real value in millimeters. The model length is calculated according to the green line in Fig.: 6.2.

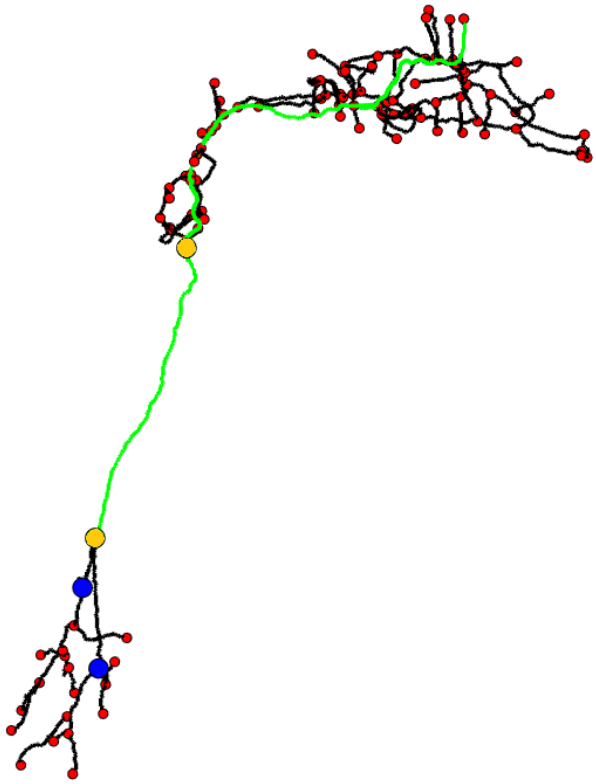

Fig. 6.2: Depiction of skeleton and key-points. Green line: computation of model length, Yellow points: trachea start and end-points, Blue points: bronchi end-points, Red dots: individual skeleton branches or end-points.

Trachea length

The trachea is extracted from the segmented mask between the points detected in the skeleton (same as in trachea volume parameter). The length of the trachea (and bronchi) is computed in two manners. Idealized and real length.

- Idealized length - This value is reflected by the euclidean distance between starting and end-point. This manner considers analysed object (trachea; bronchus) as a straight line. The analysed object is actually not really straight. The trachea is curved and distorted because it follows the curvature of the spine [51]. Bronchi are curved according to the lung structure. Idealized length provides information about the curvature of the analysed object.
- Real length - The real length of the analysed object considers mentioned curvature. All voxels in skeleton representing trachea are extracted, and the Euclidean distance is always computed between two adjacent voxels. The resulting sum of these distances reflects the real trachea length.

Bronchi length

Primary bronchi are in the network graph detected based on knowledge of the trachea end-point location node. This node includes three connected links-trachea, left and right primary bronchi. For left and right primary bronchi is this node considered as its' starting point. In the next step, end-points for these bronchi are detected. These end-points are located in the further primary bronchi branching to bronchioles. Primary bronchi classification into right and left primary bronchus is based on the anatomical knowledge that left bronchus is always longer than the right one. Both types of lengths, real and idealized, are calculated.

Trachea diameter

To calculate the diameter of the trachea, it is assumed that the trachea has a cylindrical shape. The volume and length are already computed by the algorithm. Thus the diameter can be computed as a diameter of the cylinder. The cylindrical shape is assumed because trachea has approximately the same diameter along its whole length. The cylindrical shape is also assumed most often in semirealistic model construction.

Bronchi diameter

The computation process of the bronchi diameter is identical as the computation of trachea diameter. Both bronchi are considered as cylinders, and the diameter is computed based on the knowledge of diameter and length of these objects. The narrowing of bronchi is very small in this infants age and thus is not considered in the computation.

Trachea curvature

The value expresses the extent of the trachea curvature. This parameter is computed based on the ratio of idealized and real tracheal length. In the similar manner is also computed the curvature of both main bronchi, but this parameter is not such significant in pulmonary modelling. Bronchi are shorter than trachea, and its' curvature does not influence the final shape of the representative model. The results of trachea and bronchi curvature computation are denoted in appendix B.

The computational time of the evaluating algorithm is in the range of 180 - 250 seconds. The duration depends especially on the volume of the original data, which differ according to a particular dataset. The algorithm was tested on a laptop with processor Intel core i5 6300HQ, 2,3 GHz, 8 GB RAM. It only takes over half of the computational time to import the resampled volumetric data.

6.2 Developement of representative model

The proposed parameters were evaluated independently at all created models by the evaluation algorithm. Consequently, the average value of these measured parameters is computed. Analysed results with the average value are depicted in Tab. 6.1. This average value defines a representative airway model of a newborn at stated gestational age based on these three measurements. More statistic parameters related to the measured parameters are depicted in appendix A.

Tab. 6.1: Resulting evaluation parameters:

	Model 1	Model 2	Model 3	Average
Model volume [mm^3]	4409.1	4214.9	3857.7	4160.6
Upper airways volume [mm^3]	3441.4	2921.9	2619.7	2994.3
Lower airways volume [mm^3]	967.7	1292.9	1238.0	1166.2
Trachea volume [mm^3]	566.2	760.2	914.4	746.9
Model length [mm]	145.4	124.8	114.8	128.3
Trachea length [mm]	49.3	44.5	49.7	47.8
LMB length [mm]	20,3	20,2	22.4	21.0
RMB length [mm]	11,5	10,4	8.2	10.0
Trachea diameter [mm]	1.91	2.33	2.42	2.22
LMB diameter [mm]	2.08	2.67	2.91	2.55
RMB diameter [mm]	2.14	2.57	3.84	2.85
Trachea curvature [mm]	1.23	1.19	1.17	1.20

** LMB=Left Main Bronchus, RBM=Right Main Bronchus. Trachea, LMB and RMB lengths correspond to the Real length measurement described above.*

For better visualization of the results, the standardized graph, including all analysed parameters, was created. The depiction of these wide-range values with different units is possible by standardization of all values by the standard deviation. The resulting value is given as a z-score, computed according to the formula 6.1, where the new value is obtained by subtracting the mean μ of a particular variable from its original value and dividing by the standard deviation σ of this variable.

$$Z = \frac{(X - \mu)}{\sigma} \tag{6.1}$$

The z-score variables have zero mean and variance equal to one. Z-score expresses how many standard deviations is the given value of the variable deviated from the mean value. Results of the analysis calculated as a Z-score are depicted in Fig. 6.3.

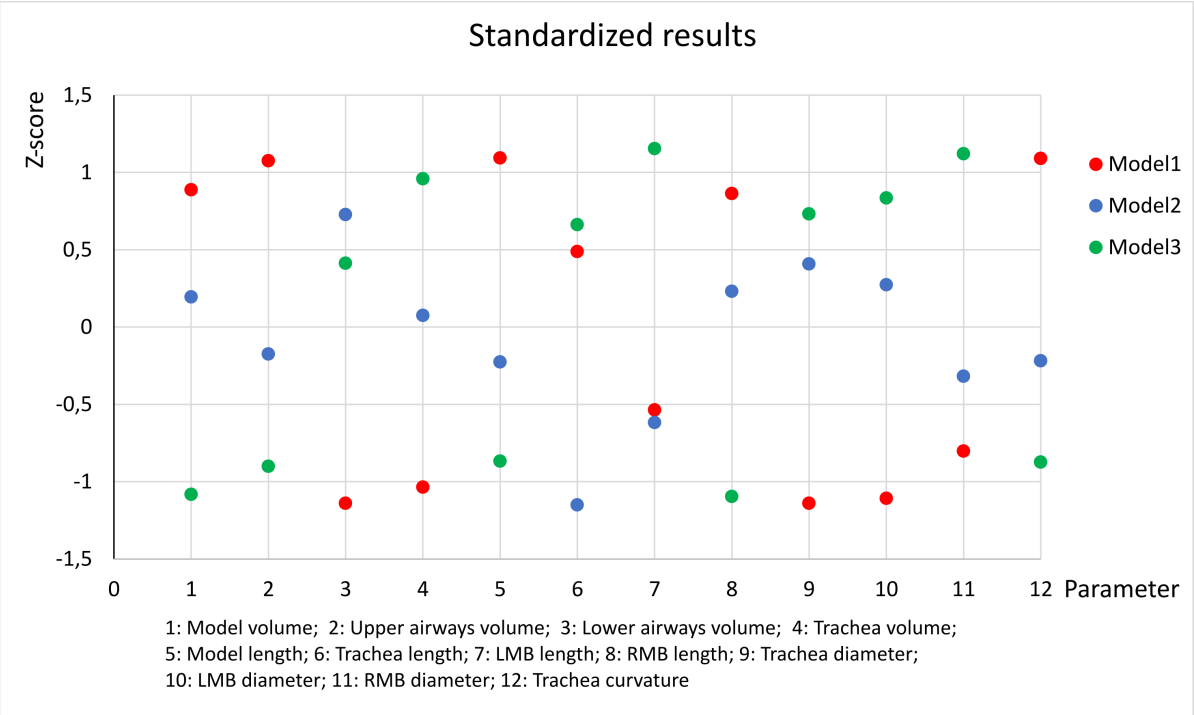

Fig. 6.3: Graph of results analysis. X-axis: individual evaluating parameters, Y-axis: standard deviation, zero value on Y-axis = average value

The graph denotes how every created model contributes to the final representative model. The first parameter in the graph is the total volume of the models. The total volume of model 3 is significantly lowest. This fact is mainly given due to the low volume of upper airways because the volume of the lower airways is closest to the average. This fact may also be related to the female sex of the newborn (Models 1 and 2 are male sex).

The shape and volume of the upper respiratory tract is the most significant parameter for air flow measurement by airway models. In this part of the airways, the pressure field of inhaled aerosols is the greatest and inhaled particles are mixed in the nasopharynx. Thus, the nasopharynx shape and volume influence the flow rate velocity in this part of the airways. The upper airways volume is highest in model 1, where the nasal cavity is wider than by other models. Thanks to the wider nasal cavity, the pressure field of the inhaled air is more uniform. Potential CPAP ventilation via nasal cannulas is, therefore, less dangerous for damage to the upper respiratory tract tissue.

The lower airways volume consist of tracheal and bronchi volume. The volume is mainly influenced by trachea volume, which is higher than the bronchi volume. Based on the results, the dependence of the tracheal volume on the lower airway

volume is evident. Both (tracheal and lower airways) volumes are lowest in model 1. In model 2 is lower airways volume highest, although the trachea volume is very close to the average value. This is due to the better segmentation of additional bronchi generation. Because of the amount of additional bronchi volume is not uniform by all models, lower airways volume is not an as significant parameter. Due to the fact that the volume of next-generations bronchi is not uniform in all models, the volume of the lower airways is not such a significant parameter. For this reason, were lower airways evaluated in individual parts in the form of trachea and bronchi evaluation. The tracheal volume is very uniformly distributed in all analysed models, which is a significant parameter for representative model characterisation.

The model length is associated with the volume of the upper airways. The shape of the nasal cavity affects the overall model length the most. Thus, the distribution of z-score in model length is identical as in upper airways volume. This parameter is very closely related to the birth weight of an infant.

The next analysed parameters were tracheal and bronchi lengths and diameters. All lengths are calculated based on the models' skeletons, which are the most accurate way to measure lengths. Based on the z-score graph observation, significant structural differences in trachea shape are visible. The trachea of model 2 is more than one standard deviation shorter compared to other models. This significant difference is given by the fact that tracheal lengths of models 1 and 3 are very similar. The length of the trachea in model 2 differs in real numbers from the average value by 3.3 millimetres, which correspond less than three voxels in original data. The short trachea length of model 2 is compensated by its diameter, which is higher than the average. In general, the trachea of model 3 is the greatest, because it has the greatest volume, is the longest, and has the largest diameter. The difference in tracheal parameters in model 3 is not significant compared to other models. This fact is balanced in the creation of a representative model by the properties of the trachea in other models.

Bronchi shape, i.e. length and diameter, were evaluated only by the main bronchi (the first generation of lower airways branching). Next bronchi branching generation is not a representative evaluating parameter, due to different segmented volume of these bronchi. The length of the left main bronchi is very similar in models 1 and 2. The length of left bronchus in model 3 looks much longer according to z-score, but in reality, it is by 2 millimetres longer than in models 1 and 2. The right main bronchus is the most extraordinary in model 3. This bronchus, compared to the other models, in model 3 is very short but thick. This shape is given by a thick transition of branching to the secondary bronchi (see Fig.: 5.5.).

The parameter which influences the overall appearance of the resulting airway model is its' overall shape. The shape of the airways is individual to every human,

and little deviations are physiological. In general, the shape of the model can be described as a curvature of the tubular structures. For this reason, real and idealized lengths of these structures were analysed to compute its' curvature. Overall curvature was calculated as a mean of the Trachea, Left and Right main bronchi curvature of each individual model. These airway parts are the most significant factor for the curved model appearance. All created models have a very similar curvature coefficient (mean=1,20). This value denotes that the models are about 20% longer due to their curved shape than if they were completely straight. The whole curvature analysis is depicted in appendix B.

The parameters of the resulting representative model are reflected the best by the average value of the analysed parameters by all three models. Each individual model contributed to the formation of the resulting representative model in a different aspect. The analysed parameters of model 2 are most often the closest to the average value, but it cannot be stated that this model corresponds to the representative one the most. In general, it is not possible to determine which of the individual models correspond to the representative one the most-all models are required to the representative model formation.

6.3 Semirealistic model geometry proposal

Based on the parameters describing the representative model, semirealistic model geometry was proposed. Several parameters of the representative model were chosen to characterise the semirealistic model. These parameters are trachea and bronchi lengths and corresponding diameters. The knowledge of these parameters suffices to create a semirealistic geometry [52]. Therefore, based on these parameters, the lower airways geometry was created. The upper airways are preserved from model 2, where the evaluated parameters corresponding to the upper airways are closest to the average value of all three models.

The whole semirealistic model development was executed in Rhinoceros, the 3D computer graphic and CAD application software. The upper airways of model 2 were imported in *.stl* format. Lower airways were modelled from geometric cylinders based on the prior knowledge of its lengths and diameters. The subcranial angle of tracheal bifurcation into main bronchi was set to 84° according to [53]. Subsequently were these cylinders converted to polygon mesh due to the connection to upper airways. The inlet to the model is also composed of a cylinder. The diameter of the cylinder is chosen so that it just fits the inflow to the nasal cavity.

Finally, the entire geometry was exported into *.stl* format, suitable for rapid prototyping (see Fig.: 6.4). Both realistic and semirealistic model geometries are suitable for different methods of characterisations and experiments. The decision to

create a semirealistic model geometry is based on the fact that the realistic models are mostly created on the basis of only one particular geometry [54].

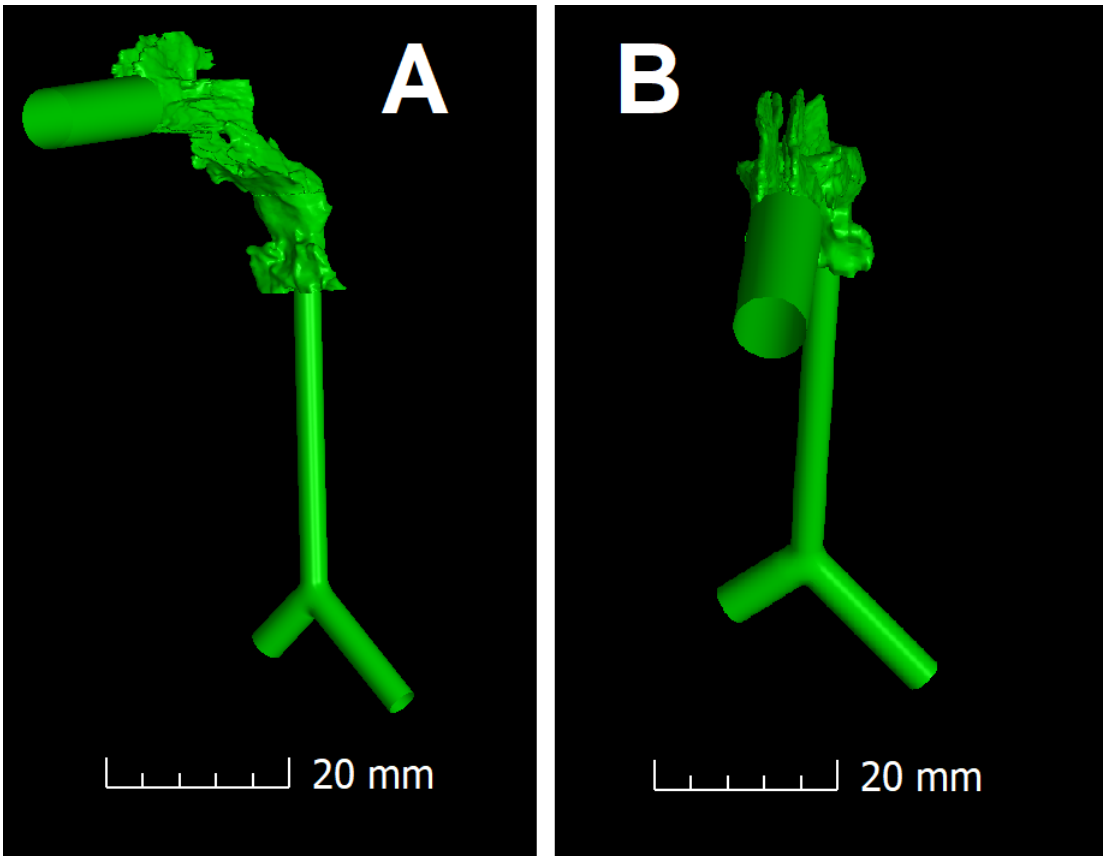

Fig. 6.4: Semirealistic model geometry proposal. (A): Frontal right view, (B): Upper frontal view

6.4 Analysis accuracy discussion

The accuracy of the final results depends on three factors. The first one is segmentation error, then the accuracy of the models' evaluation and number of particular models. The magnitude of the error given by all three factors indicates the resulting accuracy of the representative model parameters. The proposed segmentation algorithm works properly in regions with sufficient air/tissue contrast and in case of the tracheobronchial tree up to the bronchi in 1.5 mm of its' diameter. This diameter corresponds to the second generation of bronchi branching. Additional bronchi were segmented by fine manual segmentation (Fig.: 6.5). Both obtained masks are then registered to create one compact model. Thanks to the equal voxel size of both masks, no additional error could affect the model properties.

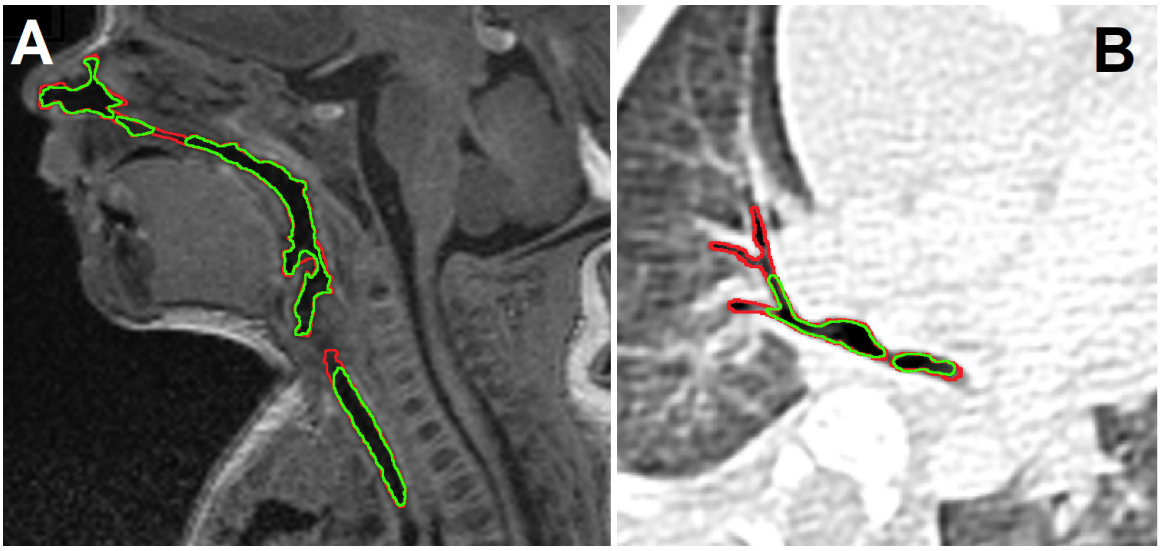

Fig. 6.5: Segmented airways: Green line - automatic segmentation by Region Growing, Red line - fine manual adjustment. (A) MRI of head - sagittal view, (B) CT of lungs - transversal view

According to the Fig.: 6.5, additional fine manual segmentation improved the real shape of the airways. The most significant impact of fine manual segmentation is in the correction of nasal cavity shape. Furthermore, the next generation of bronchi branching was added.

In order to objectively assess the impact of fine manual segmentation, Dice coefficient was calculated, according to Equation: 4.1. As a reference data were used final segmentation with manual correction. The Dice coefficient without the fine manual segmentation was computed for all three created models. The computed values are for model 1 0.722, for model 2 0.768 and for model 3 0.741. These values confirm that manual correction is important for the correct model segmentation.

The ratio of incorrectly segmented voxels to missing voxels depends on the setting of the region growing segmentation parameters. Due to insufficient air/tissue contrast in narrow parts of the airways, the threshold for maximal segmented intensity values was set relatively low to avoid leakage of the growing segment. Although the growing segment leakage detection was implemented in the algorithm, several structures in similar intensity ranges as segmented air could be wrongly added by automatic approach with a high threshold (see Fig.: 6.6). This fact leads to a bigger amount of missing voxels than wrongly segmented voxels, which are also removed by the manual correction.

The second part of the overall error of the resulting model is the accuracy of parameters evaluation. A substantial part of the model evaluation is based on its

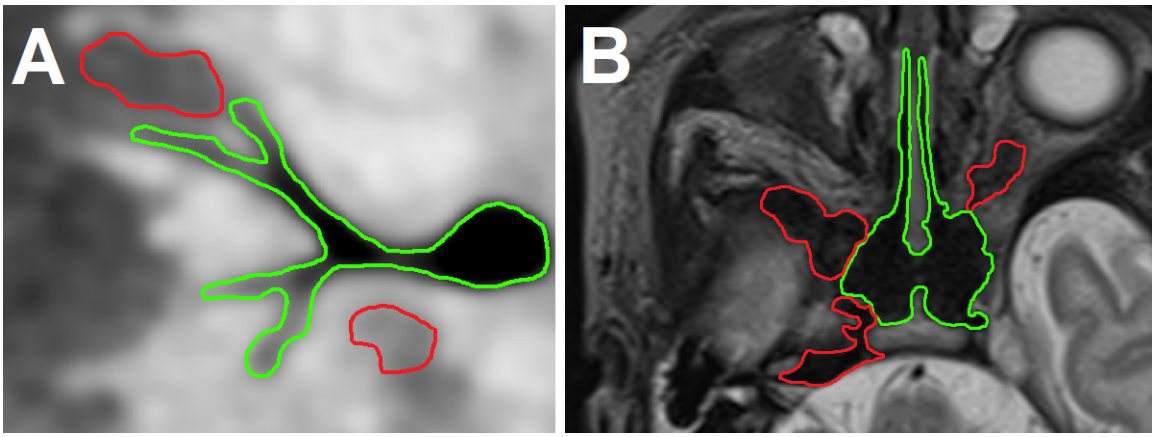

Fig. 6.6: Segmented airways: Green line - valid segmentation, Red line - Tissues or cavities which does not belong to the airways, but has similar intensity values. (A) Transversal view of lungs CT scan, (B) transversal view MRI head scan.

skeletonization. The final skeleton shape affects the overall accuracy of the evaluation. The multiple long skeleton branches occur in the upper airways. These branches characterize the shape of this part of the airways. This shape is complicated, mainly due to the tortuosity and various widths in the nasal cavity.

During the skeletonization, skeletonization artifacts arise. These artifacts take the form of false branches. False branches are caused by surface bumps or due to the thickening of the volume. For this reason, were reduced branches shorter than specified length. The threshold for the maximal branch length was set to 10 voxels. This threshold confirmed the best skeleton shape by all models. No significant structure for evaluation was removed (i.e. bronchi or larynx) but short branches were removed. This step is essential for further correct key-points detection.

As the main factor influencing the evaluation of selected parameters is correct key-points determination. These key points divide the models to particular VOIs. A robust algorithm has been developed to accurately determine the start and end-points of the trachea and bronchi. According to skeletons visualisation (Fig.: 6.7.) can be stated that these key-points are determined correctly. Consequently, the number of segmented bronchi can be observed based on the skeleton. This amount ranges within the individual models. Also, this factor influences the lower airways volume parameter.

The volume of the second and subsequent generations of bronchi is relatively low, due to their small diameter. However, the volume of these bronchi slightly affects the overall lower airways volume.

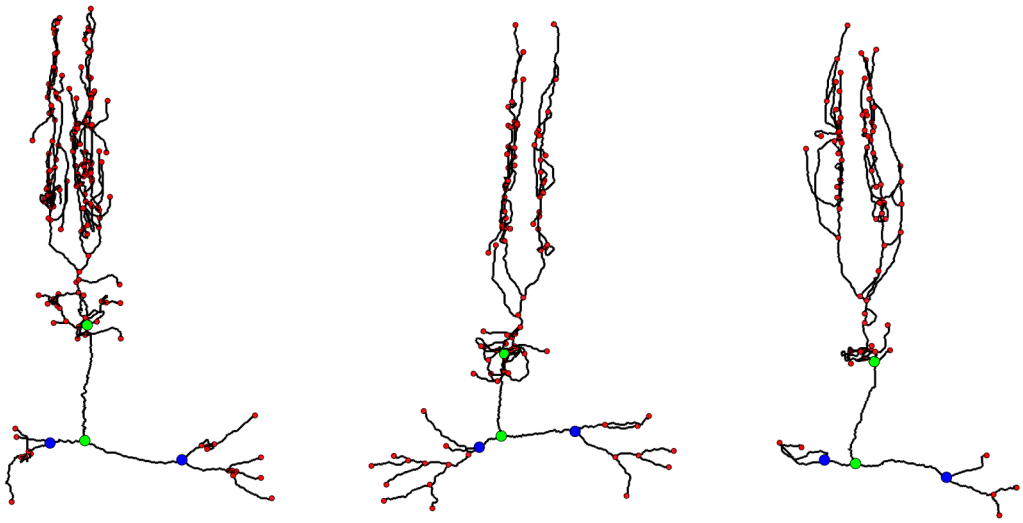

Fig. 6.7: Skeletons of analysed model: (A): Model 1, (B): Model 2, (C): Model 3. Red dots: spots of skeleton branching or skeleton endpoints, Green points: trachea start and end points, Blue: bronchioles end points.

The overall precision of the representative model description is possible to relate only to three created particular models. According to the statistical relevance of the measured data (especially standard deviation, see appendix A), the particular models describing the representative one are precise enough. However, the Shapiro-Wilk normality test shows that evaluated parameters on particular models do not have a normal distribution at 5% of significance. A representative model can therefore, only be related to these three particular models, but not to the whole population. The overall precision would improve the larger amount of the analysed models. Only three models were included in the evaluation, due to the availability of only these three neonatal tomographic datasets in this age group.

7 Conclusion

The proposed Diploma thesis deals with the development of a workflow for creating representative airway models of preterm infants. The first part of the thesis is devoted to the theoretical basis for understanding the development of the respiratory tract, including its diagnosis, imaging and available breathing support procedures. Subsequently is elaborated literary research of approaches for airway segmentation and pulmonary modelling with its applications.

Based on available datasets, suitable data for airway models creation were chosen. According to the proposed algorithm, the data were firstly pre-processed to get better segmentation results. After segmentation were combined data of upper airways with data of lower airways to obtain one particular continuous model. The segmentation was executed separately for the upper and lower respiratory tract. The segmentation works automatically with necessary manual correction. These individual segmented datasets were consequently registered into the whole respiratory tract, excluding an oral cavity. Registration was executed manually facilitated with automatic pre-alignment. The final relative position of both datasets was chosen according to the primary bronchi location, and maximal stair-step artifact reduction. Proposed dataset combination is necessary, because no dataset containing both – upper and lower airways, was available to this study. According to this approach, three airway models, based on six different infants data were created. All three models are corresponding to the infant born in 30. week of gestation and scanned approximately two weeks after birth.

All three created models were subsequently analysed by the proposed algorithm. Twelve parameters, related to the airway anatomy, were chosen for the analysis. The analysis is based on the binary masks of particular models. The models were diversified into individual VOIs based on the skeleton analysis. In skeletonized data were detected tracheal start and end-points and primary bronchi end-points, which are the key-points for the model diversification. The individual parameters are evaluated either globally on the whole model and in particular VOIs.

The final task of these Master's thesis is a description of a representative infants airways model. This representative model is based on the proposed three particular models parameters. These parameters were averaged, where the average value of each analysed parameter describes the representative model. Thus, the resulting parametric model corresponds to the airway geometry of characteristic two weeks old infant born in 30^{th} week of gestation. Based on this parametrical model was proposed a semirealistic geometry. This geometry is composed of cylinders representing the lower airways. The upper airways were preserved from the particular model 2, which correspond to the representative model the best. Finally, the geometry was exported

into *.stl* format, suitable for rapid prototyping.

The final part of the thesis is devoted to the statistical analysis. Based on the standard deviation of particular evaluated parameters, three models are enough to create one representative model. The representativeness of the final model could be increased by including more datasets of the infants. Unfortunately, this data is intricately to obtain, especially at a certain gestational age and with sufficient image quality.

Bibliography

[1] BURRI, P H. *Fetal and Postnatal Development of the Lung. Annual Review of Physiology* [online]. 1984, 46(1), 617-628. DOI: 10.1146/annurev.ph.46.030184.003153. ISSN 0066-4278. Retrieved from: <http://www.annualreviews.org/doi/10.1146/annurev.ph.46.030184.003153>

[2] HILL, Mark. *Embryology Respiratory System Development* [online]. UNSW CRICOS, 2019. ISBN 978 0 7334 2609 4. Retrieved from: <https://embryology.med.unsw.edu.au/embryology/index.php/Respiratory_System_Development>

[3] DESAI, Tushar J., Douglas G. BROWNFIELD a Mark A. KRASNOW. Alveolar progenitor and stem cells in lung development, renewal and cancer. Nature [online]. 2014, 507(7491), 190-194 [accessed 2019-10-08]. DOI: 10.1038/nature12930. ISSN 0028-0836. Retrieved from: <http://www.nature.com/articles/nature12930>

[4] BORON, Walter F. a Emile L. BOULPAEP. Medical physiology: a cellular and molecular approach. 2nd ed., International ed. Philadelphia, PA: Saunders/Elsevier, c2009. ISBN 978-141-6031-154.

[5] SCHONHAUT, L., I. ARMIJO a M. PEREZ. Gestational Age and Developmental Risk in Moderately and Late Preterm and Early Term Infants. PEDIATRICS [online]. 2015, 135(4), e835-e841. DOI: 10.1542/peds.2014-1957. ISSN 0031-4005. Retrieved from: <http://pediatrics.aappublications.org/cgi/doi/10.1542/peds.2014-1957>

[6] HUTCHINSON, Rudolf. *development of larynx, trachea and bronchi* [online]. In:. [accessed. 2019-10-12]. Amended from: <https://slideplayer.com/slide/9748839>

[7] Human embryology. 18.1 Phases of lung development [online]. University of Fribourg Amended from: <http://www.embryology.ch/anglais/rrespiratory/phasen01.html>

[8] LEE, Kuo-Sheng a Cheng-Chien YANG. Tracheal Length of Infants under Three Months Old [online]. 2016, 110(3), 268-270. DOI: 10.1177/000348940111000312. ISSN 0003-4894. Retrieved from: <http://journals.sagepub.com/doi/10.1177/000348940111000312>

[9] ROSE WILSON, PHD, MSN, RN, IBCLC, AHN-BC, CHT, Debra. MedicalNewsToday. How do babies breathe in the womb? [online]. Healthline

Media UK Limited Carrick House, Lypiatt Road, Cheltenham, Gloucestershire, England, 2017 [accessed 2019-10-30]. Retrieved from: <https://www.medicalnewstoday.com/>

[10] GUSTAFSON, Kathleen M., John J.B. ALLEN, Hung-wen YEH a Linda E. MAY. Characterization of the fetal diaphragmatic magnetomyogram and the effect of breathing movements on cardiac metrics of rate and variability. Early Human Development [online]. 2011, 87(7), 467-475. DOI: 10.1016/j.earlhumdev.2011.03.012. ISSN 03783782. Retrieved from: <https://linkinghub.elsevier.com/retrieve/pii/S0378378211001538>

[11] KOOS, Brian J., Arezoo RAJAEE, Hung-wen YEH a Linda E. MAY. Fetal Breathing Movements and Changes at Birth. Advances in Fetal and Neonatal Physiology [online]. New York, NY: Springer New York, 2014, 2014-6-7, 87(7), 89-101. Advances in Experimental Medicine and Biology. DOI: 10.1007/978-1-4939-1031-18. ISBN 978-1-4939-1030-4. ISSN 03783782. Retrieved from: <http://link.springer.com/10.1007/978-1-4939-1031-1_8>

[12] HILLMAN, Noah H., Suhas G. KALLAPUR a Alan H. JOBE. Physiology of Transition from Intrauterine to Extrauterine Life. Clinics in Perinatology [online]. 2012, 39(4), 769-783. DOI: 10.1016/j.clp.2012.09.009. ISSN 00955108. Retrieved from: <https://linkinghub.elsevier.com/retrieve/pii/S0095510812001054>

[13] New England Journal of Medicine [online]. 1967, 276(7) [accessed. 2019-11-05]. ISSN 0028-4793. Retrieved from: <http://www.nejm.org/doi/abs/10.1056/NEJM196702162760701>

[14] Alveoli depiction, [accessed. 2019-11-05], Amended from: <https://ib.bioninja.com.au/_Media/alveolus_med.jpeg>

[15] GOMELLA, TL, et al. Neonatology : Management, Procedures, On-Call problems, Diseases, and Drugs. 6. Edition. Lange, 2009. s. 416-421. ISBN 978-0-07-154431-3

[16] DAVIDSON, Lauren a Sara BERKELHAMER. Bronchopulmonary Dysplasia: Chronic Lung Disease of Infancy and Long-Term Pulmonary Outcomes. Journal of Clinical Medicine [online]. 2017, 6(1). DOI: 10.3390/jcm6010004. ISSN 2077-0383. Retrieved from: <http://www.mdpi.com/2077-0383/6/1/4>

[17] Rennie JM. Roberton's textbook of neonatology. 4th ed. Philadelphia: Elsevier; 2005.

[18] HAUT, Cathy. Pediatric Noninvasive Ventilation. Journal of Pediatric Intensive Care [online]. 2015, 04(02), 121-127. DOI: 10.1055/s-0035-1556754. ISSN 2146-4618. Retrieved from: <http://www.thieme-connect.de/DOI/DOI?10.1055/s-0035-1556754>

[19] AL-LAWAMA, Manar, Haitham ALKHATIB, Zaid WAKILEH, Randa ELQAISI, Ghada ALMASSAD, Eman BADRAN a Tyler HARTMAN. Bubble CPAP therapy for neonatal respiratory distress in level III neonatal unit in Amman, Jordan: a prospective observational study. International Journal of General Medicine [online]. 2019, 12(02), 25-30. DOI: 10.2147/IJGM.S185264. ISSN 1178-7074. Retrieved from: < https://www.dovepress.com/bubble-cpap-therapy-for-neonatal-respiratory-distress-in-level-iii-neo-peer-reviewed-article-IJGM>

[20] Wilkinson DJ, Andersen CC, Smith K, Holberton J. Pharyngeal pressure with high-flow nasal cannulae in premature infants. J Perinatol. 2008;28:42-7.

[21] ÁLVARES, Beatriz Regina, Inês Carmelita Minniti Rodrigues PEREIRA, Severino Aires de ARAÚJO NETO a Emerson Taro Inoue SAKUMA. Achados normais no exame radiológico de tórax do recém-nascido. Radiologia Brasileira [online]. 2006, 39(6), 435-440. DOI: 10.1590/S0100-39842006000600012. ISSN 0100-3984. Retrieved from: <http://www.scielo.br/scielo.php?pid=S0100-39842006000600012&script=sci_arttext&tlng=en>

[22] KAK, Avinash C., Malcolm SLANEY a Ge WANG. Principles of Computerized Tomographic Imaging. Medical Physics. 2002, 29(1), 107-107. DOI: 10.1118/1.1455742. ISSN 00942405.

[23] WANG, Ge, Yangbo YE a Hengyong YU. Approximate and exact cone-beam reconstruction with standard and non-standard spiral scanning. Physics in Medicine and Biology [online]. 2007, 52(6), R1-R13. DOI: 10.1088/0031-9155/52/6/R01. ISSN 0031-9155. Amended from: <https://www.elynspublishing.com/journal/article/opportunities-for-fluorochlorozirconate-and-other-glass-ceramic-detectors-in-medical-imaging-devices>

[24] GUILLERMAN, R. Paul. Imaging of Childhood Interstitial Lung Disease. Pediatric Allergy, Immunology, and Pulmonology [online]. 2010, 23(1), 43-68. DOI: 10.1089/ped.2010.0010. ISSN 2151-321X. Retrieved from: <http://www.liebertpub.com/doi/10.1089/ped.2010.0010>

[25] BIEDERER, J., C. HEUSSEL, M. PUDERBACH a M. WIELPUETZ. Functional Magnetic Resonance Imaging of the Lung. Seminars in Respiratory and Critical Care Medicine [online]. 2014, 35(01), 074-082 DOI: 10.1055/s-0033-1363453. ISSN 1069-3424. . Retrieved from: <http://www.thieme-connect.de/DOI/DOI?10.1055/s-0033-1363453>

[26] CIET, Pierluigi, Harm A. W. M. TIDDENS, Piotr A. WIELOPOLSKI, Jim M. WILD, Edward Y. LEE, Giovanni MORANA a Maarten H. LEQUIN. Magnetic resonance imaging in children: common problems and possible solutions for lung and airways imaging. Pediatric Radiology [online]. 2015, 45(13), 1901-1915. DOI: 10.1007/s00247-015-3420-y. ISSN 0301-0449. Retrieved from: <http://link.springer.com/10.1007/s00247-015-3420-y>

[27] GE places miniature neonatal MRI prototype in U.K. [online]. UK: AuntMinnieEurope, 2017 [accessed. 2019-12-25]. Retrieved from: <https://www.auntminnieeurope.com/index.aspx?sec=sup&sub=mri&pag=dis&ItemID=613938>

[28] HORSFIELD, K, G CUMMING, Kate KOSMAC, et al. Morphology of the bronchial tree in man. Journal of Applied Physiology [online]. 1968, 24(3), 373-383. DOI: 10.1152/jappl.1968.24.3.373. ISSN 8750-7587. Retrieved from: <https://www.physiology.org/doi/10.1152/jappl.1968.24.3.373>

[29] SCHMIDT, Andreas, Stephan ZIDOWITZ, Andres KRIETE, Thorsten DENHARD, Stefan KRASS a Heinz-Otto PEITGEN. A digital reference model of the human bronchial tree. Computerized Medical Imaging and Graphics [online]. 2004, 28(4), 203-211. DOI: 10.1016/j.compmedimag.2004.01.001. ISSN 08956111. Retrieved from: <https://linkinghub.elsevier.com/retrieve/pii/S0895611104000187>

[30] KOULLAPIS, P., S.C. KASSINOS, J. MUELA, et al. Regional aerosol deposition in the human airways: The SimInhale benchmark case and a critical assessment of in silico methods. European Journal of Pharmaceutical Sciences [online]. 2018, 113, 77-94. DOI: 10.1016/j.ejps.2017.09.003. ISSN 09280987. Retrieved from: <https://linkinghub.elsevier.com/retrieve/pii/S0928098717304992>

[31] QI, Shouliang, Baihua ZHANG, Yueyang TENG, et al. Transient Dynamics Simulation of Airflow in a CT-Scanned Human Airway Tree: More or Fewer Terminal Bronchi? Computational and Mathematical Methods in Medicine [online]. 2017, 2017, 1-14. DOI: 10.1155/2017/1969023. ISSN 1748-670X. Retrieved from: <https://www.hindawi.com/journals/cmmm/2017/1969023/>

[32] KEREKES, Attila, Attila NAGY, Miklós VERES, István RIGÓ, Árpád FARKAS a Aladár CZITROVSZKY. In vitro and in silico (IVIS) flow characterization in an idealized human airway geometry using laser Doppler anemometry and computational fluid dynamics techniques. Measurement [online]. 2016, 90, 144-150. DOI: 10.1016/j.measurement.2016.04.063. ISSN 02632241. Retrieved from: <https://linkinghub.elsevier.com/retrieve/pii/S0263224116301294>

[33] Proceedings of the Institution of Mechanical Engineers, Part H: Journal of Engineering in Medicine [online]. 2015, 229(10) [accessed. 2019-12-30]. ISSN 0954-4119. Retrieved from: <http://journals.sagepub.com/doi/10.1177/0954411915600005>

[34] SHI, Hongjian, William C. SCARFE, Allan G. FARMAN, D. SCHWASS, J. E. CATER a M. C. JERMY. Upper airway segmentation and dimensions estimation from cone-beam CT image datasets. International Journal of Computer Assisted Radiology and Surgery [online]. 2006, 1(3), 177-186. DOI: 10.1007/s11548-006-0050-8. ISSN 1861-6410. Retrieved from: <http://link.springer.com/10.1007/s11548-006-0050-8>

[35] OTSU, Nobuyuki. A Threshold Selection Method from Gray-Level Histograms. IEEE Transactions on Systems, Man, and Cybernetics [online]. 1979, 9(1), 62-66. DOI: 10.1109/TSMC.1979.4310076. ISSN 0018-9472. Retrieved from: <http://ieeexplore.ieee.org/document/4310076/>

[36] KABALIUK, N., A. NEJATI, C. LOCH, D. SCHWASS, J. E. CATER a M. C. JERMY. Strategies for Segmenting the Upper Airway in Cone-Beam Computed Tomography (CBCT) Data. Open Journal of Medical Imaging [online]. 2017, 07(04), 196-219. DOI: 10.4236/ojmi.2017.74019. ISSN 2164-2788. Retrieved from: <http://www.scirp.org/journal/doi.aspx?DOI=10.4236/ojmi.2017.74019>

[37] BUI, Nhat Linh, Sim Heng ONG, Kelvin Weng Chiong FOONG, D. SCHWASS, J. E. CATER a M. C. JERMY. Automatic segmentation of the nasal cavity and paranasal sinuses from cone-beam CT images. International Journal of Computer Assisted Radiology and Surgery [online]. 2015, 10(8), 1269-1277. DOI: 10.1007/s11548-014-1134-5. ISSN 1861-6410. Retrieved from: <http://link.springer.com/10.1007/s11548-014-1134-5>

[38] Kullback S, Leibler RA (1951) On information and sufficiency. Ann Math Stat 22(1):79–86

[39] LIU, Jianguo, Jayaram K. UDUPA, Dewey ODHNERA, Joseph M. MCDONOUGH, Raanan ARENS a M. C. JERMY. System for Upper Airway Segmentation and Measurement with MR Imaging and Fuzzy Connectedness. Academic Radiology [online]. 2003, 10(1), 13-24. DOI: 10.1016/S1076-6332(03)80783-3. ISSN 10766332. Retrieved from: <https://linkinghub.elsevier.com/retrieve/pii/S1076633203807833>

[40] WANI, Tariq M., Bruno BISSONNETTE, Mahmoud RAFIQ MALIK, Don HAYES, Archana S. RAMESH, Mazen AL SOHAIBANI a Joseph D. TOBIAS. Age-based analysis of pediatric upper airway dimensions using computed tomography imaging. Pediatric Pulmonology [online]. 2016, 51(3), 267-271. DOI: 10.1002/ppul.23232. ISSN 87556863. Retrieved from: <http://doi.wiley.com/10.1002/ppul.23232>

[41] DE NUNZIO, G, TOMMASI, E, AGRUSTI A, et al. Automatic Lung Segmentation in CT Images with Accurate Handling of the Hilar Region. Journal of Digital Imaging. 2011, 24(1), 11-27. DOI: 10.1007/s10278-009-9229-1. ISSN 0897-1889.Retrieved from: <http://link.springer.com/10.1007/s10278-009-9229-1>

[42] STYNER, Martin A., Elsa D. ANGELINI, Syed Ahmed NADEEM, Dakai JIN, Eric A. HOFFMAN a Punam K. SAHA. An iterative method for airway segmentation using multiscale leakage detection [online]. 2017-2-24. DOI: 10.1117/12.2254507. Retrieved from: <http://proceedings.spiedigitallibrary.org/proceeding.aspx?doi=10.1117/12.2254507>

[43] YUN, Jihye, Jinkon PARK, Donghoon YU, et al. Improvement of fully automated airway segmentation on volumetric computed tomographic images using a 2.5 dimensional convolutional neural net. Medical Image Analysis [online]. 2019, 2017-2-24, 51, 13-20. DOI: 10.1016/j.media.2018.10.006. ISSN 13618415.Retrieved from: <https://linkinghub.elsevier.com/retrieve/pii/S1361841518308508>

[44] ZOU, Kelly H., Simon K. WARFIELD, Aditya BHARATHA, et al. Statistical validation of image segmentation quality based on a spatial overlap index1. Academic Radiology. 2004, 11(2), 178-189. DOI: 10.1016/S1076-6332(03)00671-8. ISSN 10766332. Retrieved from: <https://linkinghub.elsevier.com/retrieve/pii/S1076633203006718>

[45] ADIBELLI, Zehra Hilal, Murat SONGU a Hamit ADIBELLI. Paranasal Sinus Development in Children: A Magnetic Resonance Imaging Analysis [online].

2011, 25(1), 30-35. DOI: 10.2500/ajra.2011.25.3552. ISSN 1945-8924. Retrieved from: <http://journals.sagepub.com/doi/10.2500/ajra.2011.25.3552>

[46] Vijaya, G., and A. Suhasini. "An adaptive preprocessing of lung CT images with various filters for better enhancement." Academic Journal of Cancer Research 7.3 (2014): 179-184. DOI: 10.5829/idosi.ajcr.2014.7.3.84231. ISSN 1995-8943 Retrieved from: <https://pdfs.semanticscholar.org/dca3/9c25c5495b710b86a637a8bba74ad736cb81.pdf>

[47] PARIS, Sylvain. A gentle introduction to bilateral filtering and its applications. In: ACM SIGGRAPH 2007 courses. 2007. p. 3-es.. Retrieved from: <https://people.csail.mit.edu/sparis/bf_course/course_notes.pdf>

[48] regionprops3. www.mathworks.com [online]. [accessed. 2020-04-05]. Retrieved from: <https://uk.mathworks.com/help/images/ref/regionprops3.html

[49] Kollmannsberger, Kerschnitzki et al., "The small world of osteocytes: connectomics of the lacuno-canalicular network in bone." New Journal of Physics 19:073019, 2017.

[50] Dijkstra, E. W. "A Note on Two Problems in Connexion with Graphs." Numerische Mathematik. Vol. 1, Number 1, 1959, pp. 269–271.

[51] NAVRÁTIL, Leoš. Vnitřní lékařství pro nelékařské zdravotnické obory. 2. Praha: Grada Publishing, 2017. ISBN 978-80-271-0210-5.

[52] LÍZAL, F. Experimentální výzkum transportu a depozice aerosolů v dýchacím traktu člověka. Brno: Vysoké učení technické v Brně, Fakulta strojního inženýrství, 2012. 137 s. Vedoucí dizertační práce prof. Ing. Miroslav Jícha, CSc.

[53] HEREK, Duygu, Ozkan HEREK a Furkan UFUK. Tracheobronchial Angle Measurements in Children: An Anthropometric Retrospective Study With Multislice Computed Tomography. Clinical and Experimental Otorhinolaryngology [online]. 2017, 10(2), 188-192. DOI: 10.21053/ceo.2016.00185. ISSN 1976-8710. Retrieved from: <http://www.e-ceo.org/journal/view.php?doi=10.21053/ceo.2016.00185>

[54] LIZAL, F, ELCNER J, K HOPKE, P, JEDELSKY, J a JICHA, M. Development of a realistic human airway model. Proceedings of the Institution of MechanicalEngineers, Part H: Journal of Engineering in Medicine. 2011, 226(3), 197-207. DOI: 10.1177/0954411911430188. ISSN 0954-4119. Retrieved from: <http://journals.sagepub.com/doi/10.1177/0954411911430188>

List of symbols, physical constants and abbreviations

MRI Magnetic Resonance Imaging
X–Ray CT X–Ray Computed Tomography
CPAP Continuous Positive Airway Pressure
IRDS Infant Respiratory Distress Syndrome
BPD Bronchopulmonary Dysplasia
HRCT High-Resolution Computed Tomography
ALARA As Low As Reasonably Achievable
CFD Computational Fluid Dynamics
STL Standard Tessellation Language
VOI Volume of Interest

List of appendices

A Complete results for representative model creation

A.1 Complete results with standard deviation

Tab. A.1: Results of the parameters evaluation:

	Model 1	Model 2	Model 3	Average	STD
Model volume [mm^3]	4409.1	4214.9	3857.7	4160.5	279.6
Upper air. volume [mm^3]	3441.4	2921.9	2619.7	2994.3	415.6
Lower air. volume [mm^3]	967.7	1292.9	1238.0	1166.2	174.1
Trachea volume [mm^3]	566.2	760.2	914.4	746.9	174.5
Model length [mm]	145.4	124.8	114.8	128.3	15.6
Trachea length [mm]	49.3	44.5	49.7	47.8	2.87
LMB length [mm]	20,3	20,2	22.4	21.0	1.24
RMB length [mm]	11,5	10,4	8.2	10.0	1.69
Trachea diameter [mm]	1.91	2.33	2.42	2.22	0.28
LMB diameter [mm]	2.08	2.67	2.91	2.55	0.43
RMB diameter [mm]	2.14	2.57	3.84	2.85	0.88
Trachea curvature [mm]	1.23	1.19	1.17	1.20	0.03
Ideal. trachea length [mm]	40	37.34	42.4	39.91	2.53
Ideal. LMB length [mm]	16.75	16.90	18.30	17.32	0.85
Ideal. RMB length [mm]	8.94	8.46	7.05	8.15	0.98

** LMB=Left Main Bronchus, RBM=Right Main Bronchus, Ideal=idealized length measurement*

A.2 Z-score analysis

Tab. A.2: Z-score analysis:

	Model 1	Model 2	Model 3	Range	Minimum	Maximum	Shapiro-Wilk Normality test
Model volume [mm^3]	0.89	0.19	-1.08	1.97	-1.08	0.89	0.68
Upper air. volume [mm^3]	1.08	-0.1	-0.90	1.98	-0.90	1.08	0.71
Lower air. volume [mm^3]	-1.14	0.73	0.41	1.87	-1.14	0.73	0.30
Trachea volume [mm^3]	-1.04	0.08	0.96	2.00	-1.04	0.96	0.87
Model length [mm]	1.09	-0.23	-0.87	1.96	-0.87	1.09	0.62
Trachea length [mm]	0.49	-1.15	0.66	1.81	-1.15	0.66	0.17
LMB length [mm]	-0.54	-0.62	1.15	1.77	-0.62	1.15	0.08
RMB length [mm]	0.86	0.23	-1.10	1.96	-1.10	0.86	0.62
Trachea diameter [mm]	-1.14	0.41	0.73	1.87	-1.14	0.73	0.31
LMB diameter [mm]	-1.11	0.27	0.84	1.94	-1.11	0.84	0.54
RMB diameter [mm]	-0.80	-0.32	1.12	1.92	-0.80	1.12	0.47
Trachea curvature [mm]	1.09	-0.22	-0.87	1.96	-0.87	1.09	0.64

B Curvature evaluation

Overall curvature was calculated as a mean of the Trachea, Left and Right main bronchi for each individual model. The mean and std values in the "overall curvature" row stand for total mean and standard deviation curvature computed from the data from all the models (see appendix A). The Tab. A.1 contains these parameters, including the average value, that describes the overall curvature of the resulting model.

Tab. B.1: Models curvature analysis:

Curvature analysis	Model 1	Model 2	Model 3	Average	STD
Trachea	1.23	1.19	1.17	1.20	0.03
Left main bronchus	1.22	1.20	1.22	1.21	0.01
Right main bronchus	1.28	1.23	1.16	1.22	0.06
Overall curvature	1.24	1.21	1.18	1.21	0.03